Time-dependent, wind-driven flow over a shallow midshelf submarine bank

J. A. Barth, S. D. Pierce, and R. M. Castelao
College of Oceanic and Atmospheric Sciences, Oregon State University, Corvallis, Oregon, USA

Received 14 October 2004; revised 14 April 2005; accepted 2 May 2005; published 27 October 2005.

[1] During summer 2001, high-resolution hydrographic, velocity, and bio-optical surveys were conducted over Heceta Bank off central Oregon. North of the bank, upwelling over simple bottom topography exhibited a classic response with a midshelf, baroclinic coastal jet and upwelled isopycnals. The coastal upwelling jet follows the bank topography as it widens offshore before reaching the southern end of the bank, where the shelf break turns almost 90° back toward the coast. The ensuing adjustment involves the offshelf transport of coastal water and the material it contains. The jet meanders anticyclonically in the "lee" of the bank before resuming its equatorward path seaward of the shelf break. A pool of high-chlorophyll (>15 mg m^{-3}) near-surface water is found in the low-velocity "lee" region created by the bank. A low-temperature, high-salinity bottom water pool, supplied primarily from the south, lies over the inshore region of the bank. This bottom pool is up to 40 m thick and contains elevated levels of suspended material. By creating an east-west perturbation in the coastal upwelling front, the flow-topography interaction introduces an alongshore pressure gradient. When southward upwelling-favorable winds relax, this alongshore pressure gradient can drive flow back to the north. This leads to northward flow on the inshore side of the bank, ultimately setting up the potential for recirculation around the entire bank complex on a timescale of about 10 days. Strong northward winds during summer lead to downwelling within 15 km of the coast, accompanied by significant (>0.2 m s^{-1}) wind-driven northward currents.

Citation: Barth, J. A., S. D. Pierce, and R. M. Castelao (2005), Time-dependent, wind-driven flow over a shallow midshelf submarine bank, *J. Geophys. Res.*, *110*, C10S05, doi:10.1029/2004JC002761.

1. Introduction

[2] Wind-driven coastal upwelling in regions with relatively uniform alongshore bottom topography and a straight coastline has been extensively studied. For example, off the U.S. west coast a southward wind drives an offshore surface Ekman layer flux which is balanced by upwelling of cold, nutrient-rich water from below. In turn, an equatorward, baroclinic coastal upwelling jet is set up in geostrophic balance with the upwelled isopycnals. Off central Oregon, the core of the upwelling jet is found at mid shelf (80–100 m water depth) with summertime average near-surface velocities of 0.35 m s^{-1} and velocities in individual events in excess of 0.8 m s^{-1} [*Huyer et al.*, 1978]. Variations in the along-shelf flow are correlated for long distances (~80 km) in the alongshore direction [*Kundu and Allen*, 1976]. The observed offshore surface transport is roughly equal to the theoretical wind-driven Ekman transport if account is taken for the wind-driven momentum to penetrate below the surface mixed layer [*Lentz*, 1992]. For a typical 20 knot alongshore wind, the offshore Ekman transport distributed over a 30-m-deep layer results in a 0.06 m s^{-1} flow. The compensatory onshore flow off Oregon is found primarily in the interior of the water column [*Smith*, 1981] as can be inferred because large Burger number flows (i.e., strong stratification) tend to suppress transport in the bottom boundary layer [*Austin*, 1998].

[3] The presence of alongshore topographic variations on otherwise relatively straight continental shelves has a profound influence on coastal circulation and hence the local ecosystem. Examples of alongshore topographic features include changes in bottom topography with or without changes in coastline orientation, e.g., submarine canyons [*Hickey*, 1997] and banks [*Butman et al.*, 1982], and coastal promontories with or without changes in the bathymetry directly offshore [e.g., *Barth et al.*, 2000]. Topographic features may disrupt or redirect strong alongshore coastal jets, create regions of weaker flow in their "shadow" and lead to enhanced mixing.

[4] In this paper, we report the results of recent field work off central Oregon to determine the influence of Heceta and Stonewall Banks on the coastal upwelling system. The Heceta Bank complex (we will refer to the Heceta and Stonewall Banks region as the bank "complex" or simply the "bank") rises to over 50% of the surrounding water

0148-0227/05/2004JC002761$09.00

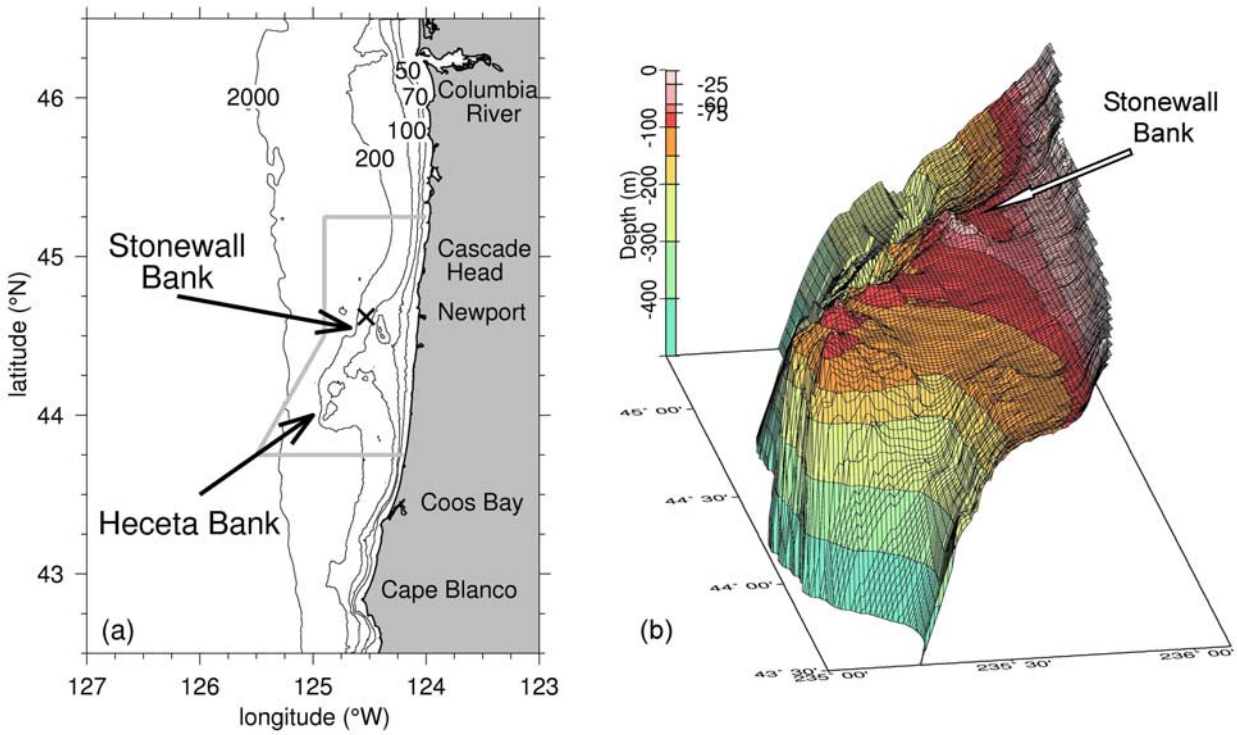

Figure 1. (a) Bottom topography off Oregon showing the locations of Heceta and Stonewall Banks. The location of National Data Buoy Center (NDBC) buoy 46050 from which winds were measured is indicated by the cross; isobaths are in meters. The gray-bordered polygon surrounding the banks indicates the region of Coastal Ocean Advances in Shelf Transport (COAST) in situ measurements. (b) Three-dimensional plot of Heceta and Stonewall Banks looking from the southwest.

column depth on the continental shelf off central Oregon (44°20′N) (Figure 1). The banks extend about 100 km in the along-shelf direction and widen the shelf to 60 km from the relatively narrow 25-km-wide shelves both to the north and south. Stonewall Bank rises to within 7 m of the ocean surface and the offshore pinnacles of Heceta Bank are 46 m deep at their shallowest. A productive fishery is associated with Heceta Bank [*Pearcy et al.*, 1989] and cold, chlorophyll-rich upwelled water has been observed well seaward of the continental shelf break south of the bank [*Barth et al.*, 2005]. Recent advances in towed, undulating vehicle capabilities have allowed rapid, high-spatial-resolution surveys of physical and bio-optical properties to be made over the continental shelf and slope. Together with shipboard acoustic Doppler current profiling (ADCP), this has made possible the exploration of three-dimensional, time-dependent processes in regions with alongshore variations in coastline geometry and/or bottom bathymetry.

[5] The results reported here are part of the Coastal Ocean Advances in Shelf Transport (COAST) project that seeks to understand and quantify cross-shelf transport and transformation processes in the strongly wind-driven coastal ocean off central Oregon [*Barth and Wheeler*, 2005]. Two intensive field efforts were conducted in summer 2001 together with coordinated ocean circulation, ecosystem and atmospheric modeling. A primary goal is to contrast the coastal ocean response in a region of relatively simple alongshore bottom topography versus that associated with a substantial submarine bank. A second objective is to determine how the hydrographic and velocity structure influences the magnitude and distribution of primary and secondary production in this region.

[6] During May–June and August 2001, two vessels conducted interdisciplinary research off central Oregon. One ship conducted rapid, high-spatial-resolution surveys of the three-dimensional thermohaline, velocity and bio-optical fields using SeaSoar and shipboard ADCP. Surface maps of nutrients and iron were also made [*Chase et al.*, 2005]. A second ship collected high-vertical-resolution cross-shelf profiles along 44.25° and 45°N of water properties: temperature, salinity and turbulence parameters from a loosely tethered microstructure profiler [*Perlin et al.*, 2005]; nutrients, carbonate species [*Hales et al.*, 2004], phytoplankton photosynthesis parameters, and particulate and dissolved organic material [*Karp-Boss et al.*, 2004] from a pumped profiling system. An instrumented aircraft measured properties of the lower atmosphere and upper ocean during and between the month-long intensive field experiments [*Bane et al.*, 2005]. A set of moorings measured physical and bio-optical parameters from May to August and a land-based radio system continuously measured surface currents hourly over a region encompassing the bank [*Kosro*, 2005]. A high-resolution, three-dimensional shelf circulation [*Gan and Allen*, 2005] and coupled

ecosystem ocean model [*Spitz et al.*, 2003], and a mesoscale atmospheric model [*Bielli et al.*, 2002] are being used to investigate the dynamics of the system.

[7] In a companion paper, *Castelao and Barth* [2005] (hereinafter referred to as CB) use the 2001 COAST SeaSoar and ADCP data sets to compute the spring and summer mean and standard deviations of hydrographic and velocity fields off central Oregon during upwelling. In the present study, time-dependent effects, circulation during wind relaxation and reversal, and the nature of the deep suspended material pool over Heceta Bank are presented and discussed. We also include results from field work in 1999 and 2000 to help illustrate the phenomenon of interest, e.g., alongshore pressure gradients and recirculation.

[8] After a description of the data collected and analysis methods, a series of horizontal maps and vertical sections of hydrographic, velocity and bio-optical properties are used to describe the coastal ocean response to wind forcing around and over the Heceta Bank complex. This is followed by an exploration of the alongshore pressure gradient created by the flow-topography interaction, a description of flow during wind relaxation and reversal, and lastly an investigation of the bottom pool over the bank. The results are then discussed by comparing them with results from other regions with alongshore topographic variations and with numerical model predictions, and by considering their impact on the coastal ecosystem. This is followed by a brief conclusions section.

2. Methods

[9] Two mapping surveys were carried out from the R/V *Wecoma* during 2001. The first, 23 May to 13 June, was intended to sample conditions early in the upwelling season while the second, 6–25 August, was targeted to sample fully developed summertime upwelling. The survey region extended 167 km alongshore from 43.75°–45.25°N encompassing the entire Heceta Bank region (Figure 1). A set of eight east-west lines were sampled from approximately the 45 m isobath (5 km or less from the coast) to out over the continental slope and adjacent deep ocean up to 90 km offshore. East-west lines were separated by an average of 24 km in the north-south direction and each survey took an average of 2.2 days to complete. Several of the survey lines, e.g., the Newport Hydrographic Line (44.65°N) and 44.0°N, were chosen to line up with historical sampling transects [*Huyer et al.*, 2002]. Lines over the Heceta-Stonewall Bank region were chosen to avoid passing over the shallow peaks of those submarine features. During each cruise, this "big box" sampling region was occupied four or five times, alternating with higher-spatial-resolution surveys centered near the COAST southern (44.25°N) and northern (45°N) intensive sampling lines. The majority of the results presented here are from the big box surveys.

[10] The average 24 km between-track spacing during the big box surveys was chosen as a compromise between a desire for coherent sampling in the alongshore direction and the goal to complete the big box map in approximately 2 days. The former is justified for physical variables (temperature, salinity, velocity) by previous studies in this region, e.g., 80 (35) km alongshore correlation length scales for along-shelf (cross-shelf) velocity over the midshelf [*Kundu and Allen*, 1976]. Wind and water velocity spectra from moorings in this region show a majority of energy in the "wind band" (2–10 days) over the shelf increasing to 25 days and longer offshore (4200 m of water) [*Huyer*, 1990] hence the approximately 2 day map duration choice.

[11] Results from similar SeaSoar mapping cruises in July 1999 and in May–June and July–August 2000 are used to place the COAST 2001 results in context. Details of the sampling, data processing and results from the 1999 experiment can be found in the work of *Barth et al.* [2001] and *Oke et al.* [2002a], while those from the 2000 surveys can be found in the work of *Barth et al.* [2005].

2.1. Winds

[12] Winds were measured at the NOAA National Data Buoy Center (NDBC) buoy 46050 located at 44.62°N, 124.53°W, approximately 37 km offshore of Newport, Oregon (Figure 1). Wind stress was calculated following the method of *Large and Pond* [1981] and then low-pass filtered using a filter with a 40 hour width at half amplitude to remove short-period (e.g., diurnal) fluctuations (Figure 2).

2.2. SeaSoar Hydrography and Chlorophyll

[13] From 23 May to 13 June (spring) and from 6 to 25 August (summer) 2001, hydrographic and bio-optical measurements were made from the towed undulating vehicle SeaSoar [*Pollard*, 1986]. SeaSoar was towed using a bare hydrographic cable and profiled from the sea surface to 115–120 m over deep water and to within 10 m of the bottom over the shelf. Cycle time in deep water was about 6.5 min resulting in surface points being separated by 1.3 km at the ship's typical 7 knot (3.6 m s^{-1}) tow speed. Horizontal separation between profiles at middepth is half this value. Cycles over the shallow shelf, 0–500 m, took 1.5 min so surface points were separated by about 300 m. Bottom avoidance was accomplished by using R/V *Wecoma*'s 3.5 kHz Knudsen echosounder as input to the SeaSoar flight control software.

[14] The SeaSoar was equipped with a Seabird 911+ conductivity-temperature-depth (CTD) instrument with pumped, dual temperature-conductivity (T/C) sensors pointing forward through the nose of SeaSoar. Details of CTD data processing can be found in the work of *Barth et al.* [2000]. A Western Environmental Technology Laboratories (WET Labs) nine-wavelength light absorption and attenuation instrument, ac-9, was mounted on top of SeaSoar in a rigid saddle and with a streamlined nose cone to minimize drag [*Barth and Bogucki*, 2000]. Water for the ac-9 was pumped from an inlet-outlet just above the CTD T/C sensors in the nose of SeaSoar. Two WET Labs FlashPak fluorometers [*WET Labs Inc.*, 1997] both equipped to measure chlorophyll fluorescence at 685 nm, but with one using blue excitation (440 nm, 30 nm bandpass) and the other using green excitation (490 nm, 30 nm bandpass), were mounted alongside the ac-9 on top of SeaSoar and received the same pumped water as the ac-9. In this paper, we report the chlorophyll content estimated from the fluorescence measured by the "green" FlashPak. Chlorophyll fluorescence obtained by the FlashPak was calibrated against laboratory fluorometric analysis of discrete samples following *Strickland and Parsons* [1972].

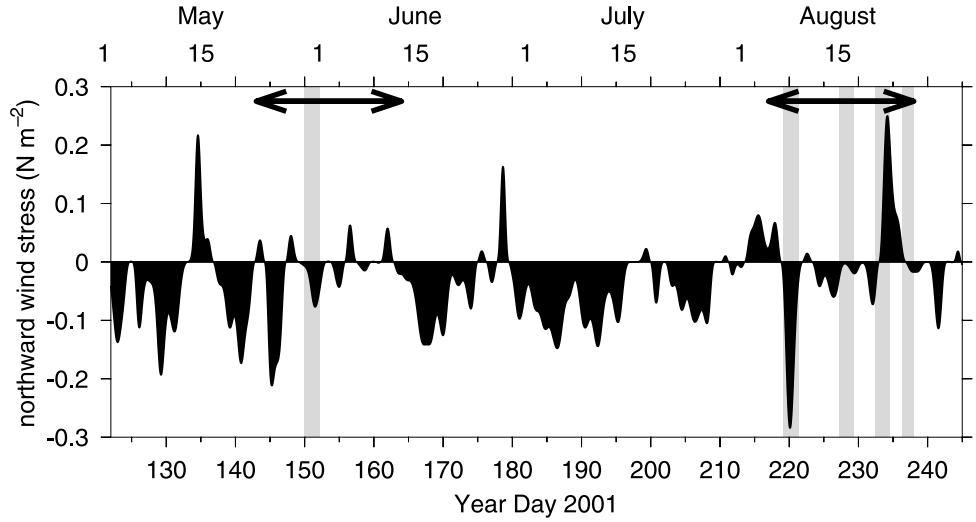

Figure 2. Wind stress calculated from winds measured at NOAA NDBC buoy 46050 off Newport, Oregon. The timing of COAST research cruises is indicated by horizontal double-ended arrows, and shaded bars denote times of individual maps.

[15] For making horizontal maps and vertical sections, the measurements were first averaged vertically to 2 dbar bins and horizontally to 1.25 km. The usual caveats about aliasing of large-scale, low-frequency hydrographic measurements by internal waves and internal tides apply, although strong coherence in the features described here suggests that these effects are small. A complete set of the SeaSoar maps and vertical sections of all parameters can be found in the work of *O'Malley et al.* [2002] and *Barth et al.* [2003].

[16] The spatially averaged temperature, salinity and pressure data are used to compute geopotential anomaly (dynamic height in meters multiplied by the acceleration of gravity) in J kg^{-1} (m^2 s^{-2}) relative to 45 db. Although a deeper reference level is desirable for estimating geostrophic currents and transport (e.g., 100, 500 or 1000 m), the 45 db reference level is sufficient for describing the location of the upwelled pycnocline and the accompanying strong equatorward jet (e.g., CB). By using the 45 db reference level, there is no need to apply an extrapolation technique across the depth-varying continental shelf and slope.

[17] Estimates of the bottom mixed layer depth are obtained by applying two criteria to the density profiles obtained with SeaSoar near the bottom. The top of the bottom mixed layer is defined where the density differs by 0.01 kg m^{-3} from the deepest observed value. In addition, a bottom mixed layer must actually be present within the range of SeaSoar observations which is determined by requiring at least 3 m of density values with a standard deviation of less than 0.0022 kg m^{-3}. Finally, estimates of the thickness of the high light attenuation bottom layer and the maximum light attenuation in that layer are obtained from near-bottom ac-9 measurements. The light attenuation at 650 nm in m^{-1}, also known as "beam-c," will be used as an estimate of suspended particulate matter. The thickness of the high-particle bottom layer is estimated by differencing the depth at which the beam-c rises 0.15 m^{-1} above the background level of the relatively clear interior water, with the local water depth as measured by the ship's echosounder.

2.3. Shipboard Current Profiles

[18] Velocity profiles along the ship track were obtained using a shipboard 153.6 kHz narrowband ADCP. Measurement ensembles were obtained every 2.5 min using a pulse length of 12 m and vertical bin size of 8 m. When water depth is less than about 450 m, bottom tracking is used to reference the ship-relative velocities to an Earth-based reference frame. In deep water, differential GPS is used for computing ship velocity. The shallowest reliable data was from 17 m. Other details of the data collection and processing follow *Barth et al.* [2000] and the complete data set can be found by *Pierce and Barth* [2002a, 2002b]. The overall error in a 5-min-averaged absolute ADCP velocity is estimated to be ±0.02 m s^{-1} when bottom tracking is available and ±0.04 m s^{-1} otherwise.

[19] For maps of ADCP velocities, each vector is a 5 km spatial average in the horizontal and 10 m in the vertical. For vertical sections, 5 min ADCP data are contoured using a Barnes objective analysis scheme with three iterations [e.g., *Daley*, 1991] where the horizontal (vertical) grid spacing is 1 km (8 m), and the successive smoothing length scales are 10 km (50m), 5 km (25 m) and 2.5 km (12.5 m). The usual caveat about aliasing low-frequency velocity fields by inertial oscillations applies, but strong coherence between the ADCP velocities and the hydrographic fields suggests that this aliasing is minimal.

[20] In most of the COAST study region, tidal currents from individual tidal constituents (e.g., M2, K1) are expected to be about 0.05 m s^{-1}, smaller than the subtidal velocity features described here. Using an array of current meters extending across the Oregon continental slope and shelf, *Torgrimson and Hickey* [1979] reported M2 (K1) semimajor axis amplitudes of 0.02–0.06 (0.02–0.04) m s^{-1}. Using a data-assimilating model together with high-frequency coastal radar and moored acoustic Doppler pro-

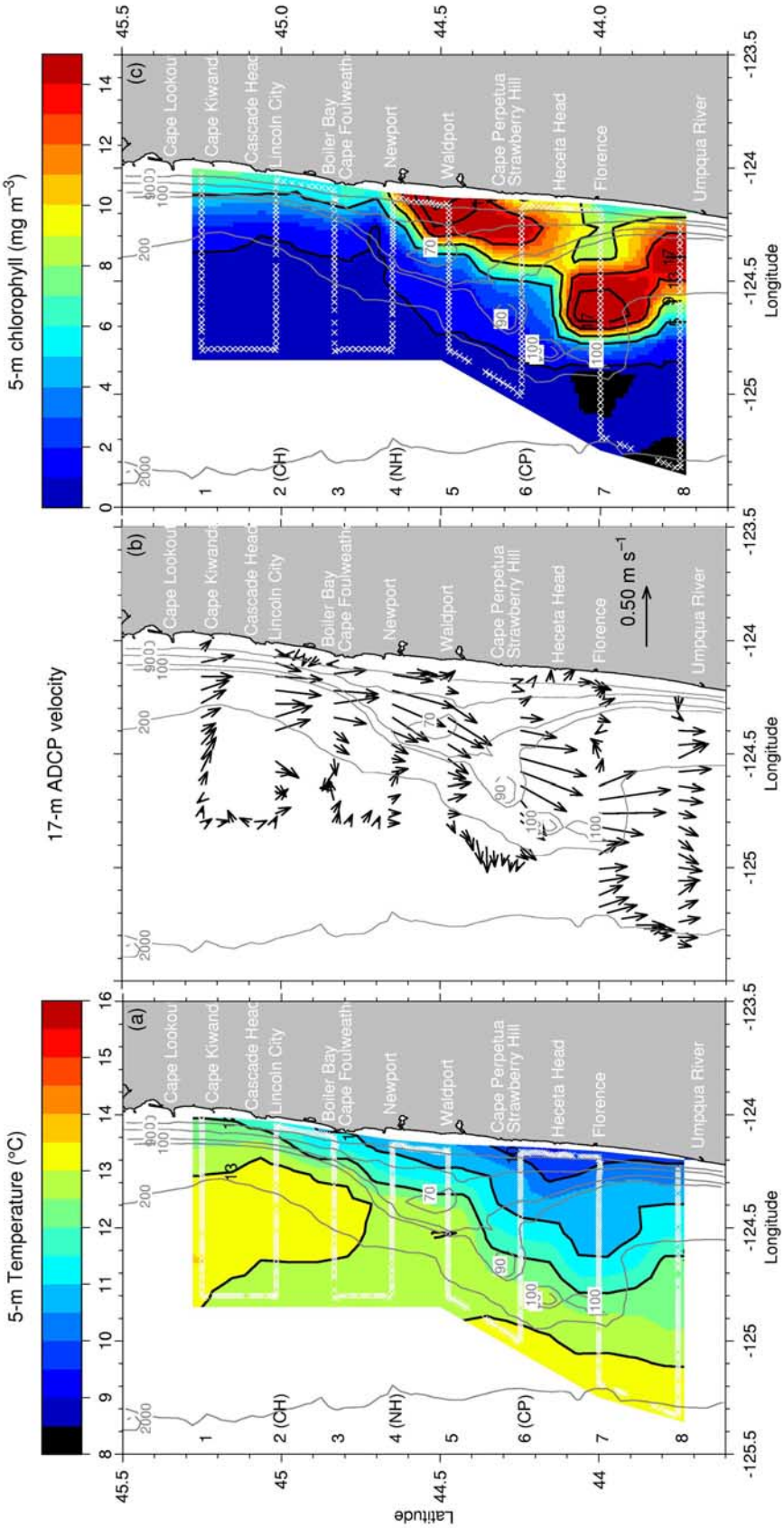

Figure 3. Maps of 5 m temperature (°C), 17 m acoustic Doppler current profiler (ADCP)-derived velocity vectors, and 5 m chlorophyll (mg m^{-3}) from 29 May to 1 June 2001. Measurements from along the ship track are shown as white dots, and east-west line labels appear at left in Figures 3a and 3c. Isobaths are in meters.

filer velocities, *Erofeeva et al.* [2003] find similar magnitudes for the M2 and K1 currents except in a region directly over Heceta Bank where K1 velocities reach 0.10 m s^{-1} through a resonance of the tide with a first-mode barotropic shelf wave. Although the tidal currents are small in most of the study region, shipboard ADCP velocities are presented after removing an estimate of the tidal motion using the *Erofeeva et al.* [2003] tidal model. After removing the barotropic tidal currents from the ADCP measurements, a baroclinic tidal signal may still be present. The baroclinic tide is challenging to estimate and highly variable in time and space, as it depends upon the density structure in the water column. Semidiurnal (M2) baroclinic tidal currents at the surface off Oregon can be as large as 0.10 m s^{-1} [*Torgrimson and Hickey*, 1979; *Kurapov et al.*, 2003].

2.4. Surface Drifters

[21] To illustrate near-surface circulation over the Heceta Bank complex, holey sock drifters were drogued at 15 m and tracked via satellite [*Niiler et al.*, 1995]. At the latitude of the study region, fixes are obtained roughly 9–12 times per day. Five surface drifters were released on 12 April 2000 from 10 (18.5) to 65 (120.4) nautical miles (km) offshore along the Newport Hydrographic (NH) line (44.65N) during a Global Ocean Ecosystem Dynamics Northeast Pacific (GLOBEC NEP) Long-Term Observation Program cruise [*Huyer et al.*, 2002]. Drifter trajectories are calculated by fitting a cubic smoothing spline [*Reinsch*, 1967] to the raw fixes, which minimizes the overall curvature while not allowing the root-mean-square deviation between the fitted and the actual locations to exceed 1 km. The GLOBEC NEP drifter data set can be found at http://diana.coas.oregonstate.edu/drift.

3. Results

[22] Wind stress during spring and summer 2001 exhibited the typical 2–10 "weather band" variability and was predominantly upwelling-favorable during the two COAST cruises (Figure 2). A strong wind reversal, i.e., winds to the north, occurred from 21 to 24 August with sustained hourly averaged winds of 25 kts and 1-min-averaged winds in excess of 35 kts. There was a period of sustained upwelling during the first half of July between the research cruises which significantly influenced the offshore location of the upwelling front and jet off central Oregon (CB). More details about the atmospheric forcing during the 2001 upwelling season can be found by *Bane et al.* [2005].

3.1. Deflection of the Upwelling Jet

[23] Coastal upwelling varies along the central Oregon coast as revealed by a map of near-surface (5 m) temperature obtained from 29 to 31 May 2001 (Figure 3a). The region of upwelling is narrow in the north where the continental shelf is narrow and bottom topography is relatively uniform. The classic coastal upwelling experiments of the 1970s took place in this region, in particular near 45.25°N, and led to a fundamental understanding of two-dimensional, wind-driven upwelling dynamics [e.g., *Huyer et al.*, 1978; *Kundu and Allen*, 1976]. A vertically sheared, equatorward coastal upwelling jet accompanies the sea surface temperature front and upwelled isopycnals (Figures 3a, 3b, 4a, and 4b). The jet carries 0.7 Sv (1 Sverdrup = 10^6 m^3 s^{-1}) to the south (CB). The inshore region in the north shows elevated values of chlorophyll around 5 mg m^{-3}, reflecting phytoplankton primary production driven by the upwelling of nutrient-rich water into the euphotic zone. A layer near the bottom with elevated light attenuation, indicative of higher amounts of suspended material, extends up to 20 m above the bottom over the entire shelf (Figure 4c). This material likely contains phytoplankton detritus sinking down from the euphotic surface layer [*Chase et al.*, 2005]. However, its signature does not show up in chlorophyll fluorescence (Figure 4d), i.e., fluorescence per unit chlorophyll has decreased, presumably because these cells have been out of the euphotic zone for some amount of time [see *Cowles et al.*, 2002].

[24] The new results from this study involve the interaction of the wind-driven coastal upwelling front and jet with alongshore bathymetric variations represented by the Heceta Bank complex. The upwelling front and jet follow the midshelf isobaths (80–100 m) to the southwest around the banks (Figure 3). The region of cold, upwelled water extends farther offshore over the banks. Early in the upwelling season, the core of the equatorward jet lies inshore of the Heceta Bank pinnacles between 44° and 44.4°N (Figure 3b), but with cumulative upwelling-favorable wind forcing the jet core moves out over and seaward of the pinnacles later in the season (Figure 4f) (CB). There is an indication that local wind-driven upwelling is occurring adjacent to the coast over the bank as evident by upwelled isopycnals and weak southward flow found there (Figures 4e and 4f). Lastly, near-surface (5 m) chlorophyll is substantially elevated (in excess of 15 mg m^{-3}) over the bank inshore of the coastal upwelling jet and front (Figure 3c).

[25] At the southern end of the bank where the shelf isobaths (<200 m) turn sharply back toward the coast, the coastal upwelling jet continues equatorward, displaced seaward of the continental shelf break. This results in a massive amount of cross-isobath or offshelf transport of water, the 0.7 Sv in the coastal upwelling jet, and the material it contains.

3.2. Inshore "Lee" Region

[26] Another new result from this study is the presence of a low-velocity region over the banks inshore of the coastal upwelling jet (Figures 3b and 4g). This "lee" region allows for a longer residence time for upwelled water, contributing to the enhanced phytoplankton levels observed there (Figure 3c). CB show that this low-velocity region is present both in the spring and summer mean circulation. A region of low velocity over the bank has also been noted in land-based radar measurements of surface currents [*Oke et al.*, 2002a; *Kosro*, 2005]. *Barth et al.* [2005] and CB noted that a longer residence time in this region leads to higher surface temperatures in late summer due to solar heating (CB, Figure 4).

[27] There is also evidence for northward flow just inshore of the coastal upwelling jet on the southern end of Heceta Bank (Figures 3b and 4f). This northward flow is part of a meander present at the southern end of the bank as the coastal upwelling jet adjusts to the rapidly changing bottom topography in this region. As the water column stretches, the jet turns cyclonically (counterclockwise) back

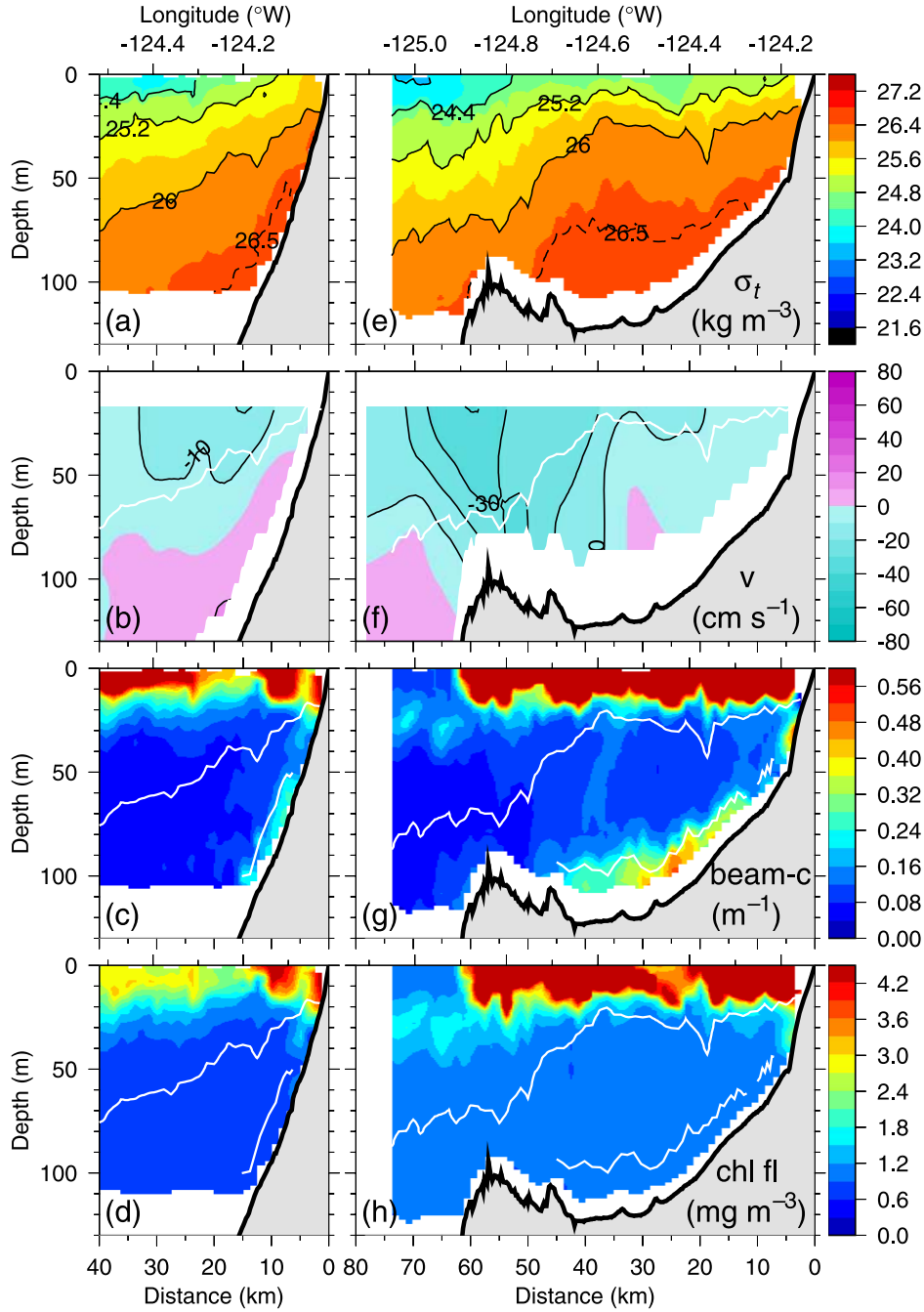

Figure 4. Cross-shelf vertical sections from (a–d) 45.02°N on 15 August 2001 and (e–h) 44.11°N on 19 August 2001 (day 231) of density (kg m^{-3}), north-south velocity (cm s^{-1}), light attenuation at 650 nm ("beam-c") (m^{-1}), and chlorophyll derived from fluorescence (mg m^{-3}). The white curve in the midwater column in the lower three rows is the 26.0 kg m^{-3} density contour. The white curve near the bottom in the lower two panels is the bottom mixed layer depth.

toward the coast in order to preserve potential vorticity. This cyclonic turning leads to the observed northward flow that, in fact, supplies deep water to the region inshore of the Heceta Bank pinnacles (CB). The cyclonically turning coastal jet encounters shallow water farther east, so then turns anticyclonically to continue its way equatorward.

[28] The lee region also contains a deep pool of elevated light attenuation that extends up to 40 m above the bottom inshore of the Heceta Bank pinnacles (Figure 4g). The high light attenuation layer extends above the bottom mixed layer into the stratified region above. This may be caused by suspended material being left behind in the stratified region during detrainment from the bottom mixed layer. The signature of the light-attenuating deep pool is not seen in chlorophyll fluorescence (Figure 4h), presumably because, as in the northern section, these cells have been out of the euphotic zone for some amount of time [see *Cowles et al.*, 2002]. This bottom material likely contains particulate

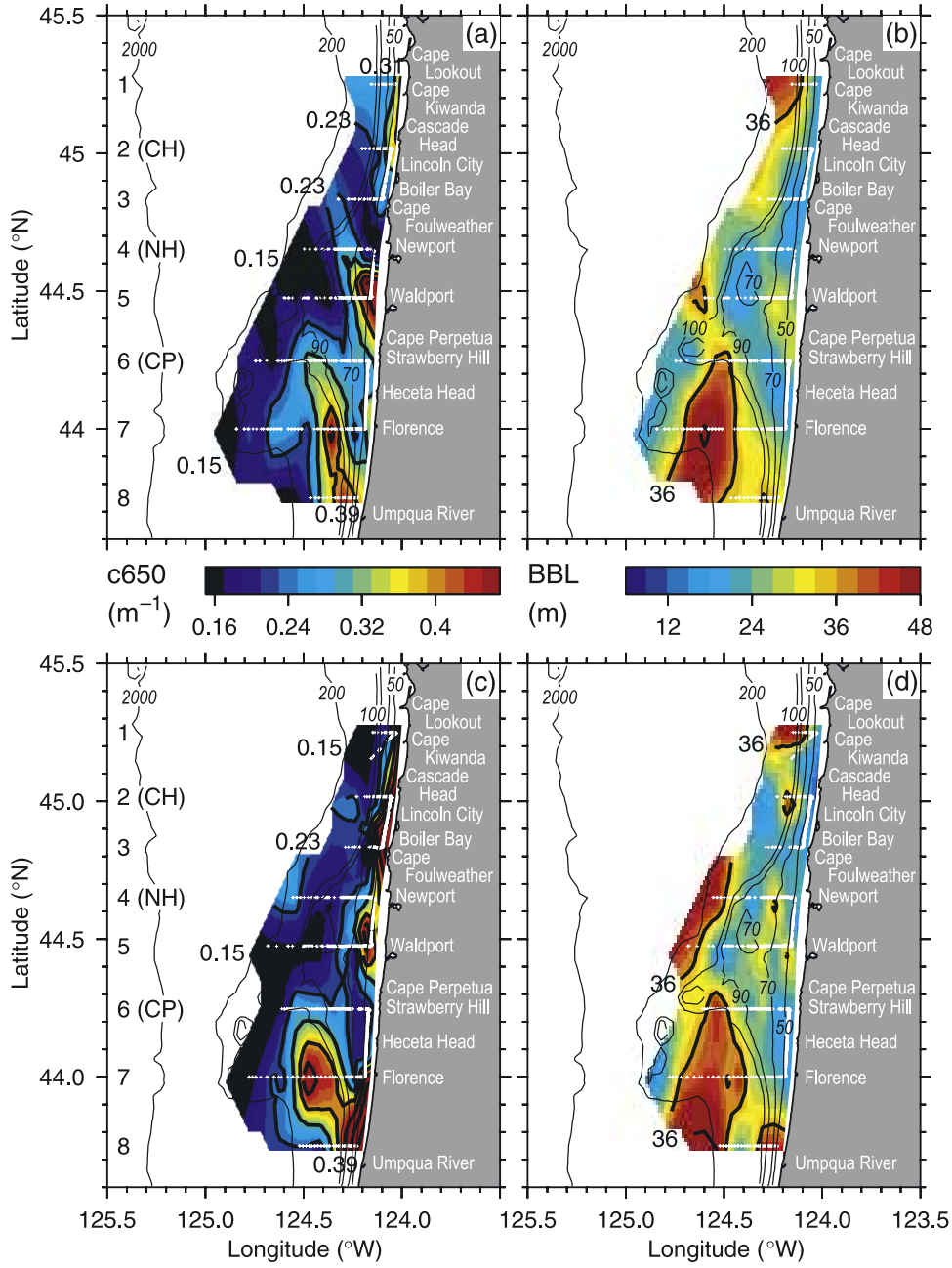

Figure 5. (a, c) Maximum light attenuation (m^{-1}) at 650 nm (c650) in the bottom boundary layer and (b, d) thickness (m) of the bottom layer during (top) 15–17 August and (bottom) 20–22 August 2001.

organic carbon rained down from the surface phytoplankton pool lying over Heceta Bank and hence could play a role in the oxygen levels found there (see section 4.2).

[29] To examine the characteristics of this bottom layer over the entire study region, the maximum value of light attenuation at 650 nm in the bottom layer and the thickness of the bottom layer are plotted for two time periods in Figure 5. For a survey conducted from 15 to 17 August 2001, after a period of weak upwelling-favorable winds (Figure 2) and preceding the sampling along 44.11°N shown in Figure 4 (right-hand column), light attenuation in the bottom layer is high nearshore in several locations (43.75°, 44.5°, and 45°N) where the layer is 20–30 m thick (Figures 5a and 5b). The most notable feature offshore is the high light attenuation region between 44°–44.25°N and 124.3°–124.5°W in the lee region of the banks. As was evident in the individual section at 44.11°N (Figure 4g), the bottom layer with high light attenuation is in excess of 30 m thick in this region. Note that the bottom layer is low in particles over the inshore flank of the Heceta Bank pinnacles, presumably because they are rocky and therefore less material is available for resuspension.

[30] A second map of light attenuation in the bottom layer during 20–22 August 2001 (Figure 5c), sampled from south to north during a change from upwelling-favorable to strong downwelling-favorable winds (Figure 2), shows a similar

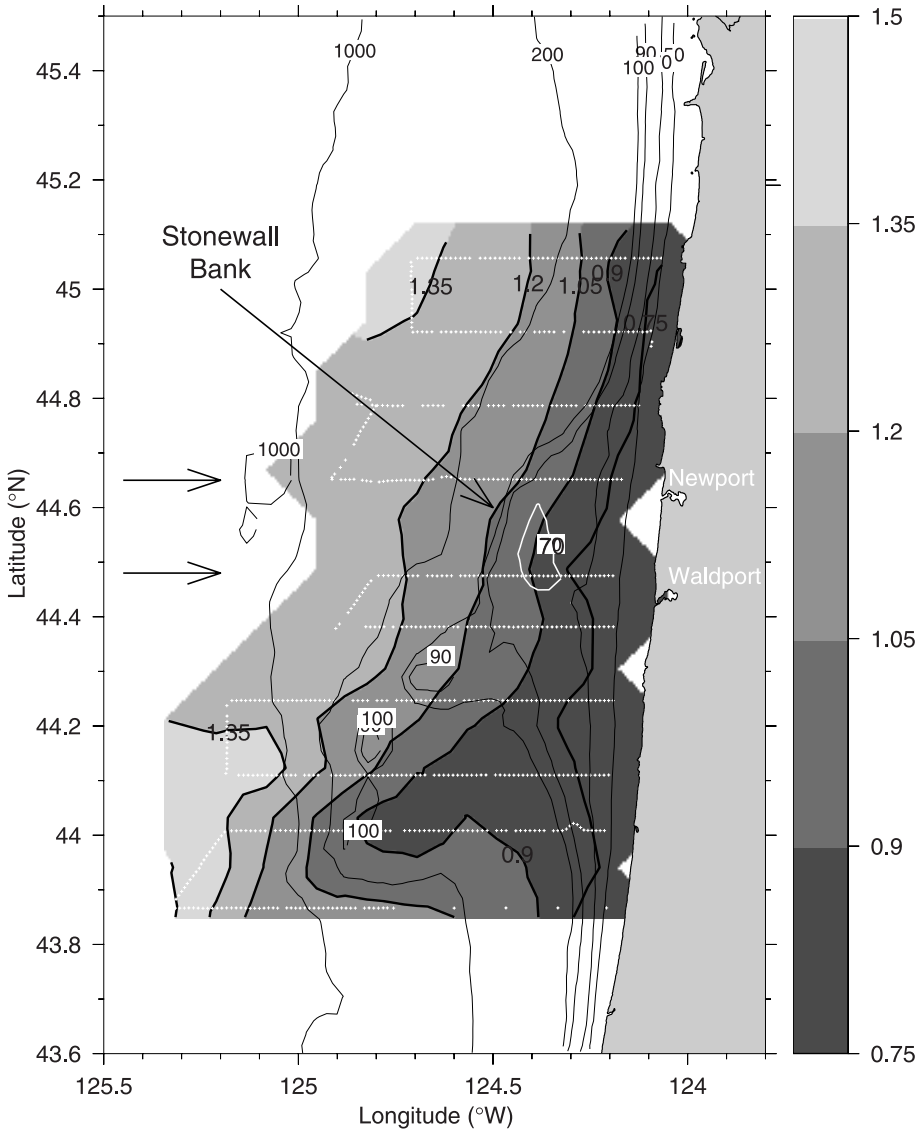

Figure 6. Geopotential anomaly (m^2 s^{-2}) at 5 m relative to 45 m during 23–26 July 1999. Data locations are indicated by white dots; isobaths are in meters. Arrows indicate locations of vertical sections shown in Figure 13.

pattern to that observed five days earlier with notable exceptions. The high light attenuation bottom layer in the lee region is still present, but now nearshore bottom layer light attenuation levels are higher than observed 5 days earlier and exist all along the coast from 44.5°N and to the north. Note that the thickness of the bottom layer (Figure 5d), both adjacent to the coast and out over the continental shelf, is now greater than 5 days earlier. Both these observations are consistent with the response to strong northward winds during the latter part of this survey. Particles are being downwelled along the shelf and the bottom layer is thickening [*Trowbridge and Lentz*, 1991] (see also section 3.5).

3.3. Alongshore Pressure Gradient

[31] By disrupting the uniformity of the alongshore, wind-driven coastal upwelling jet and front, the Heceta Bank complex induces alongshore pressure gradients which may potentially drive alongshore currents. A plot of geopotential anomaly from a survey conducted off central Oregon during 23–26 July 1999 is shown in Figure 6. The intent is not to compute geostrophic velocities or total transport which would benefit from using a deep reference level, but simply to show the location and direction of the coastal upwelling jet and front. Thus the geopotential anomaly is shown at 5 m relative to 45 m, depths sampled by SeaSoar across the entire shelf and slope. The same deflection of the upwelling jet to the southwest along the bank edge is evident in July 1999 as it was in May 2001 (Figure 3).

[32] To illustrate the alongshore pressure gradient created by the flow-topography interaction, the geopotential anomaly at a distance 20 km offshore is plotted as a function of latitude (Figure 7). A positive pressure gradient exists

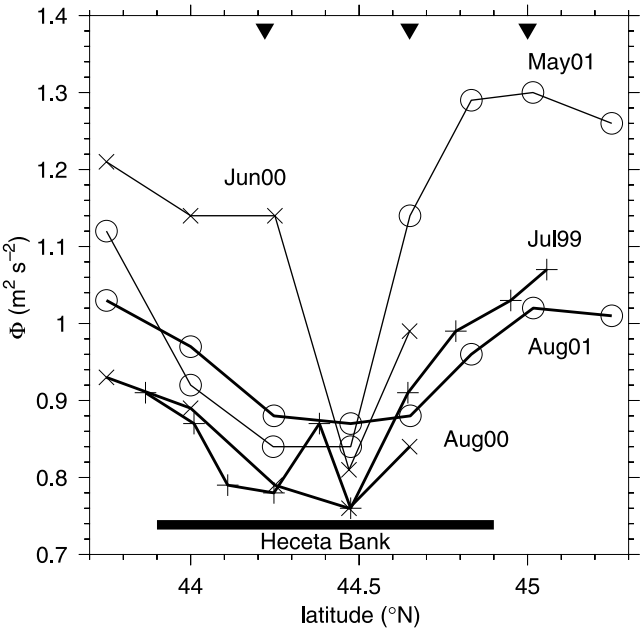

Figure 7. Geopotential anomaly (m^2 s^{-2}) at 5 m relative to 45 m as a function of latitude 20 km offshore. Data are from surveys in early summer (thin lines) (May 2001, open circles; June 2000, crosses) and late summer (bold lines) (July 1999, plusses; August 2000, crosses; August 2001, open circles). The latitudinal range of Heceta Bank is indicated, and filled triangles along the top indicate locations of moorings during summer 2001.

poleward (upstream) of Heceta Bank and is associated with offshore flow in the upwelling jet. Downstream of the bank, the alongshore pressure gradient is negative, associated with onshore flow. As shown by *Gan and Allen* [2002] and discussed further in section 4.3, this situation is balanced under constant wind forcing, but when the wind relaxes the negative pressure gradient south of the topographic feature (a cape in the work of *Gan and Allen* [2002]) becomes unbalanced and can then drive alongshore flow to the north. To show that the creation of alongshore pressure gradients occurs every upwelling season near Heceta Bank, geopotential anomalies at 20 km offshore are plotted for two surveys during the 2000 GLOBEC NEP and from the two COAST 2001 surveys (Figure 7). Note that although geopotential anomalies are larger away from the bank early in the upwelling season due to the upwelling being restricted closer to the coast, all the surveys show the creation of a minimum in geopotential anomaly associated with Heceta Bank and similar alongshore pressure gradients.

3.4. Circulation During Wind Relaxation

[33] When alongshore wind forcing goes to zero, that is, it relaxes, it is expected that the coastal upwelling jet and front will remain intact since they are in geostrophic balance. The system will eventually spin down from a combination of internal and bottom friction, and perhaps through baroclinic instability removing energy from the mean front and jet and transferring it to meanders and eddies. Note that cross-shelf transport in the surface Ekman layer also ceases during relaxation as do the compensatory interior and/or bottom boundary layer cross-shelf transports. However, the addition of a poleward pressure gradient force as set up through the flow-topography interaction described above may drive currents to the north. Vertical sections of density and north-south velocity from a period of sustained upwelling-favorable winds and during a wind relaxation are shown in Figure 8. To illustrate this typical response to relaxation, data from summer 1999 are used. A similar response occurs in spring and summer 2001 [*O'Malley et al.*, 2002; *Barth et al.*, 2003; *Pierce et al.,* 2002a, 2002b]. Note the relatively small change in the upwelled isopycnal shapes. In contrast, inshore currents and those at depth over the mid shelf (>80 m depth) are poleward. Note that the velocity difference between the shallowest and deepest measured velocity in the jet core at mid shelf (0.25 m s^{-1}) remains about the same in the two realizations, consistent via thermal wind balance with the nearly unchanged sloping isopycnals. In other words, the sheared velocity profile has been shifted by addition of a depth-independent poleward velocity such that flows are poleward near the bottom during relaxation. This description is consistent with the fact that variations from the mean baroclinic flow are barotropic [*Kundu and Allen*, 1976].

3.5. Circulation During Wind Reversal

[34] During the summer when winds are generally upwelling-favorable, there are periods when the winds are northward thus downwelling-favorable. During 21–24 August 2001, the oceanic and ecosystem response off Oregon to strong summertime downwelling was observed. During the downwelling event, northward winds lasted 3–4 days and reached speeds of up to 40 knots. The surface layer warmed by about 4°C over the entire continental shelf as warm oceanic surface water was advected onshore in a surface Ekman layer (Figure 9). Downwelled isotherms were found within 15 km of the coast (Figures 9 and 10). The narrow downward plunge of the isotherms and contours of chlorophyll concentration and buoyancy frequency over the 90 m isobath (Figures 9e, 9g, and 9h) is due to an internal soliton [*Moum et al.*, 2003], sampled but underresolved by SeaSoar. The southward upwelling jet and the accompanying tilted isopycnals that existed before the downwelling event persisted, but were located over the mid- to outer shelf (Figures 9 and 11). Northward currents in excess of 0.2 m s^{-1} were found inshore of the 70 m isobath and were continuous over the entire study region (130 km alongshore) (Figure 11). There is more vertical shear in this nearshore northward jet (Figure 9f) compared with that found during wind relaxation (Figure 8d). Lastly, vigorous wind-driven mixing leads to a nearshore region of low buoyancy frequency between the downwelled pycnocline and a thin stratified surface layer (Figure 9h). The onshore surface Ekman flux (2 m^2 s^{-1}) at the height of this downwelling event and the vertical scales (up to 15 m) of nearshore wind-driven turbulence estimated using a microstructure instrument onboard SeaSoar were reported by *Ott et al.* [2003].

[35] Prior to the downwelling event, chlorophyll fluorescence was confined to the upper 20 m (Figures 4 and 9c). During strong northward winds, high chlorophyll concen-

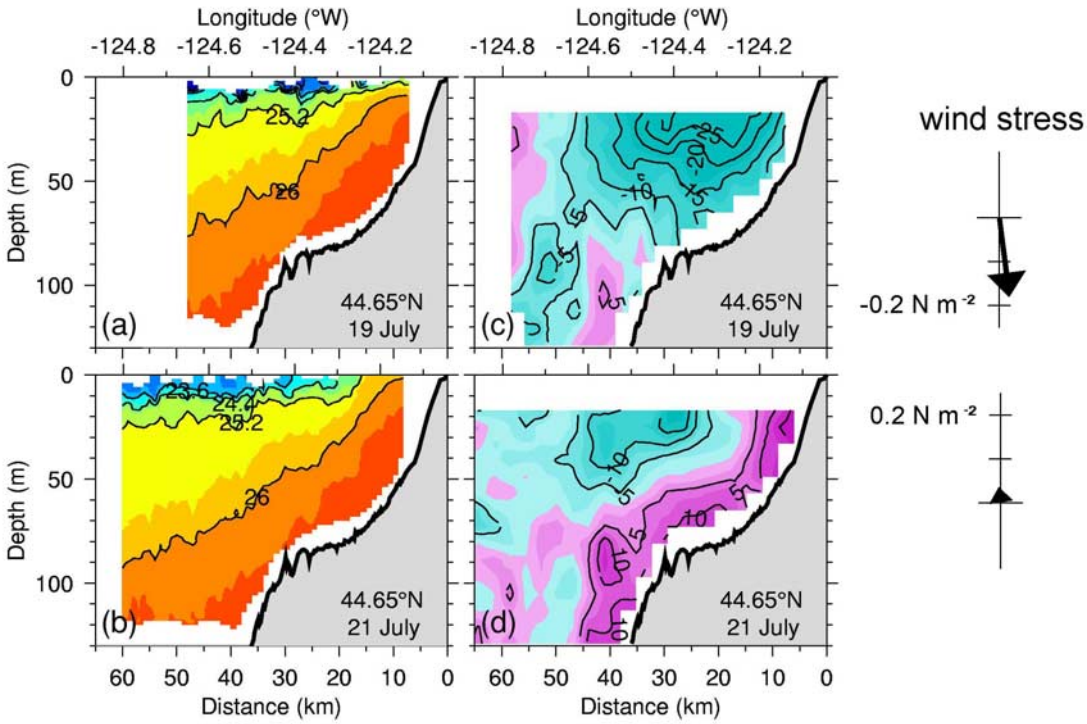

Figure 8. Vertical sections of (a, b) density (kg m^{-3}) and (c, d) north-south velocity (cm s^{-1}) along 44.65°N on (top) 19 July and (bottom) 21 July 1999. A measure of the low-pass filtered wind stress during the time of the vertical sections is indicated at right, where north is up and east is to the right.

trations were downwelled with the isopycnals near the coast and were distributed throughout the water column in water depths less than about 70 m (Figure 9g). The phytoplankton downwelled to the bottom over the shelf adjacent to the coast are responsible for the high light attenuation observed there (e.g., the northernmost three lines in Figure 5c). Strong summertime downwelling is one mechanism for transporting organic material from the euphotic zone to depth over the continental shelf.

[36] In summary, during both wind relaxation and reversal, inshore currents can reverse and flow poleward. These nearshore poleward flows are more depth-independent during wind relaxation and more vertically sheared during active downwelling, consistent with creation of downwelled isopycnals. During downwelling, surface water and the material it contains are transported shoreward and eventually downward inshore of the 50–70 m isobath.

3.6. Recirculation Around Bank

[37] Flow-topography interaction and time-dependent wind forcing combine to create the conditions for potential recirculation around the Heceta Bank complex. The scenario is as follows. The equatorward coastal upwelling jet follows the midshelf isobaths to the southwest, separating from the coast, before reaching the southern end of the bank where the jet then turns cyclonically (counterclockwise) back toward the coast. When the wind relaxes or turns to blow toward the north, water near the coast (up to ~15 km offshore) is driven northward. A water parcel could then move back northward on the inshore side of the bank complex before either transiting to the north in a downwelling jet (or possibly be driven right onto the coast depending on the presence of onshore surface Ekman transport and its distribution (see *Austin* [1998] and *Austin and Barth* [2002] for more details)) or encountering the separating coastal upwelling jet on the northern end of the bank complex. If entrained in the separating, equatorward jet, the water parcel could repeat the cycle.

[38] Evidence for recirculation around the Heceta Bank complex via the mechanisms described above is provided by near-surface drifters (Figure 12). The two drifters released off Newport (44.65°N) over the shelf are entrained in the separating coastal upwelling jet and move southwestward. Both turn (cyclonically) onshore on the southern part of the bank complex before transiting northward in response to northward wind-driven currents. One drifter (orange, Figure 12) transits to just north of its release latitude before grounding. The second (blue, Figure 12) gets entrained in the equatorward upwelling jet and repeats nearly the same path to the southern part of the bank. This circuit takes approximately 11 days. This drifter completes a cyclonic loop in the lee region of the bank before grounding on 16 May near 43.75°N.

[39] During this same period, a drifter released 120 km offshore initially gets caught up in the offshore eddy field before being forced shoreward by sustained onshore surface Ekman transport (green, Figure 12). This drifter is then entrained in the equatorward coastal upwelling jet and completes a cyclonic loop in the lee region of the bank. As discussed below, onshore surface transport during

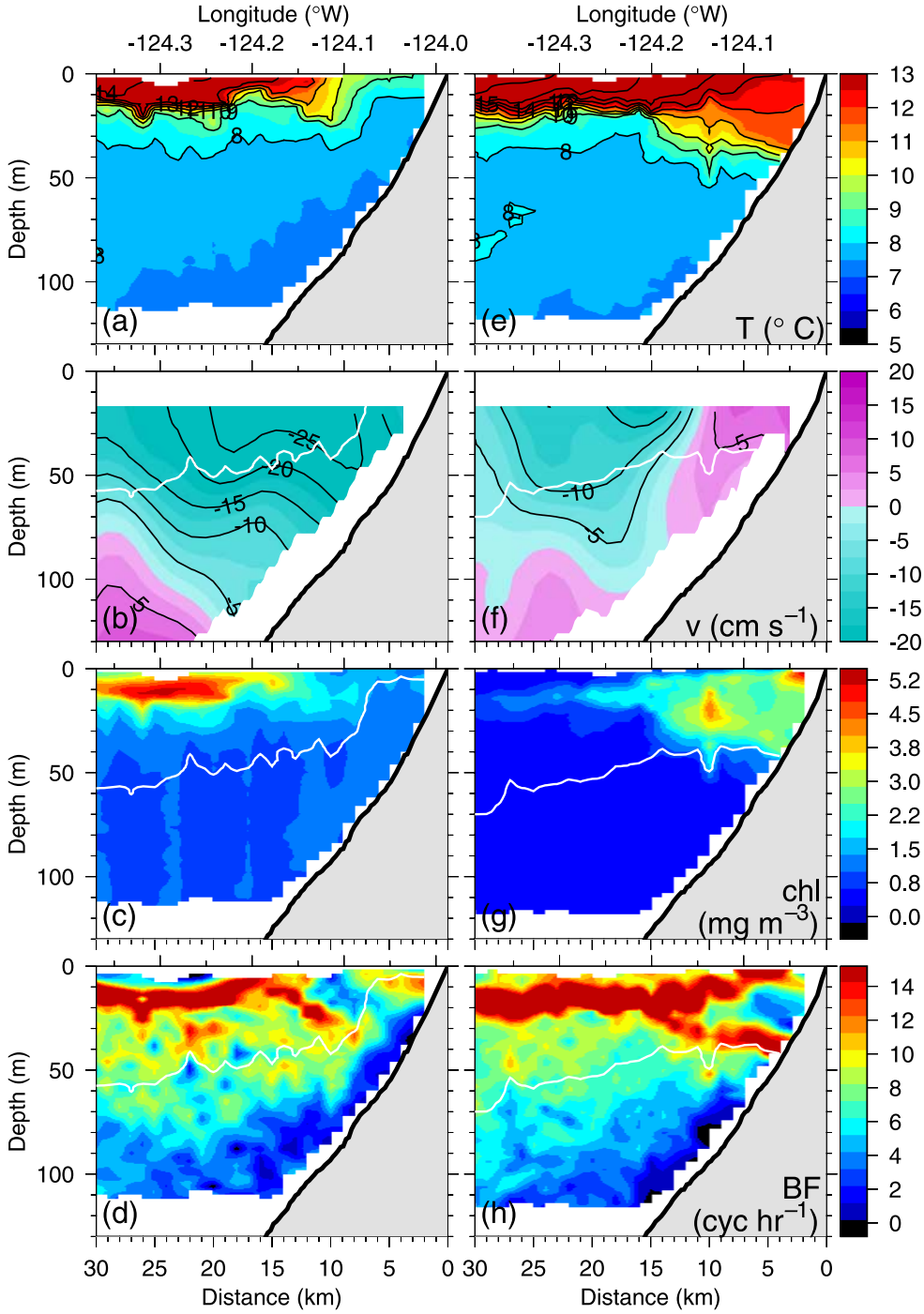

Figure 9. Vertical sections of properties measured near 45°N during (a–d) upwelling (45.11°N, 2256 UTC on 9 August 2001) and (e–h) downwelling (45.02°N, 2158 UTC on 25 August 2001) wind forcing. The 26.0 kg m^{-3} isopycnal is shown in white on plots of north-south velocity, chlorophyll, and buoyancy frequency.

downwelling can provide water and the material it contains to the Heceta Bank region.

3.7. Enhanced Mixing

[40] Evidence for enhanced mixing in the lower part of the water column due to wind-driven flow over the rough, bank topography is shown in sections obtained in July 1999 just upstream (44.65°N) and downstream (44.47°N) of Stonewall Bank (Figure 13). Currents over the shelf as measured with shipboard ADCP (not shown) were southward over the entire shelf in both sections as can be inferred from the slope of the upwelled 25.7 kg m^{-3} isopycnal. Maximum values in the equatorward upwelling jet reached 0.15–0.35 m s^{-1}. The temperature structure upstream of Stonewall Bank reveals coastal upwelling and consists of a warm surface layer, associated with fresh, Columbia River–

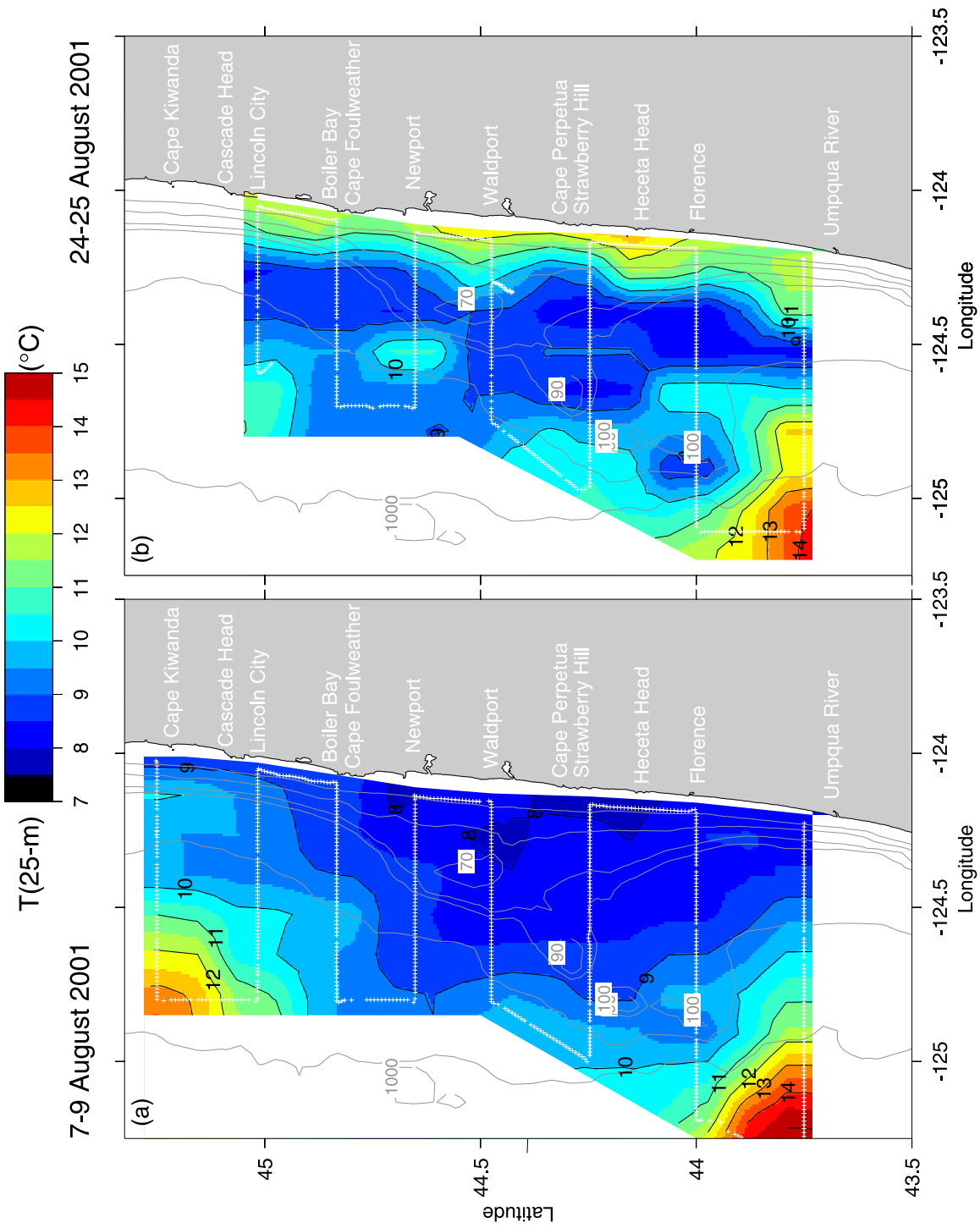

Figure 10. Maps of 25 m temperature (°C) during (a) upwelling-favorable (7–9 August 2001) and (b) downwelling-favorable (24–25 August 2001) wind forcing.

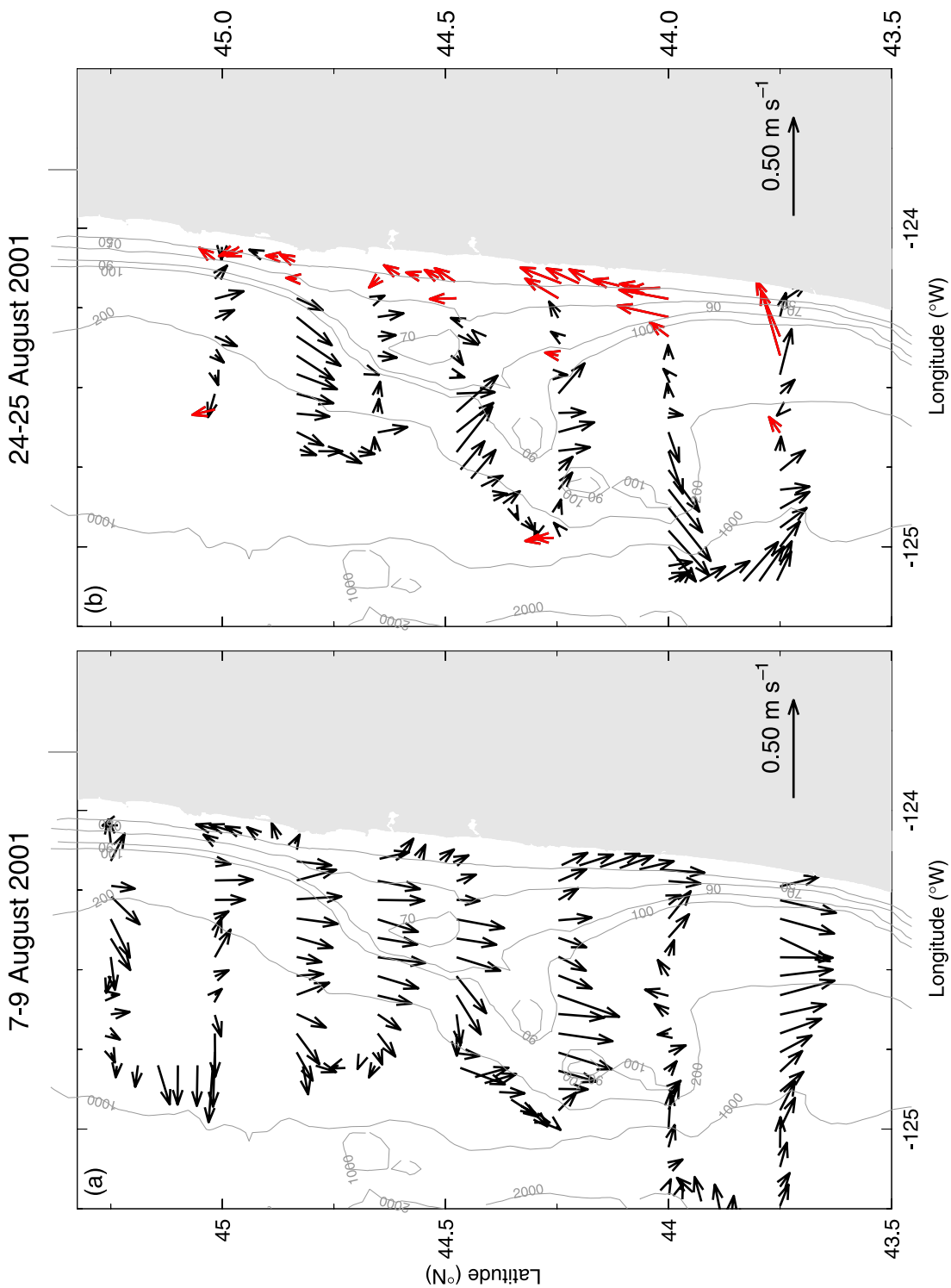

Figure 11. Velocity vectors at 25 m during (a) upwelling-favorable (7–9 August 2001) and (b) downwelling-favorable (24–25 August 2001) wind forcing. During downwelling, velocities with a northward component greater than or equal to 0.05 m s^{-1} have been colored red.

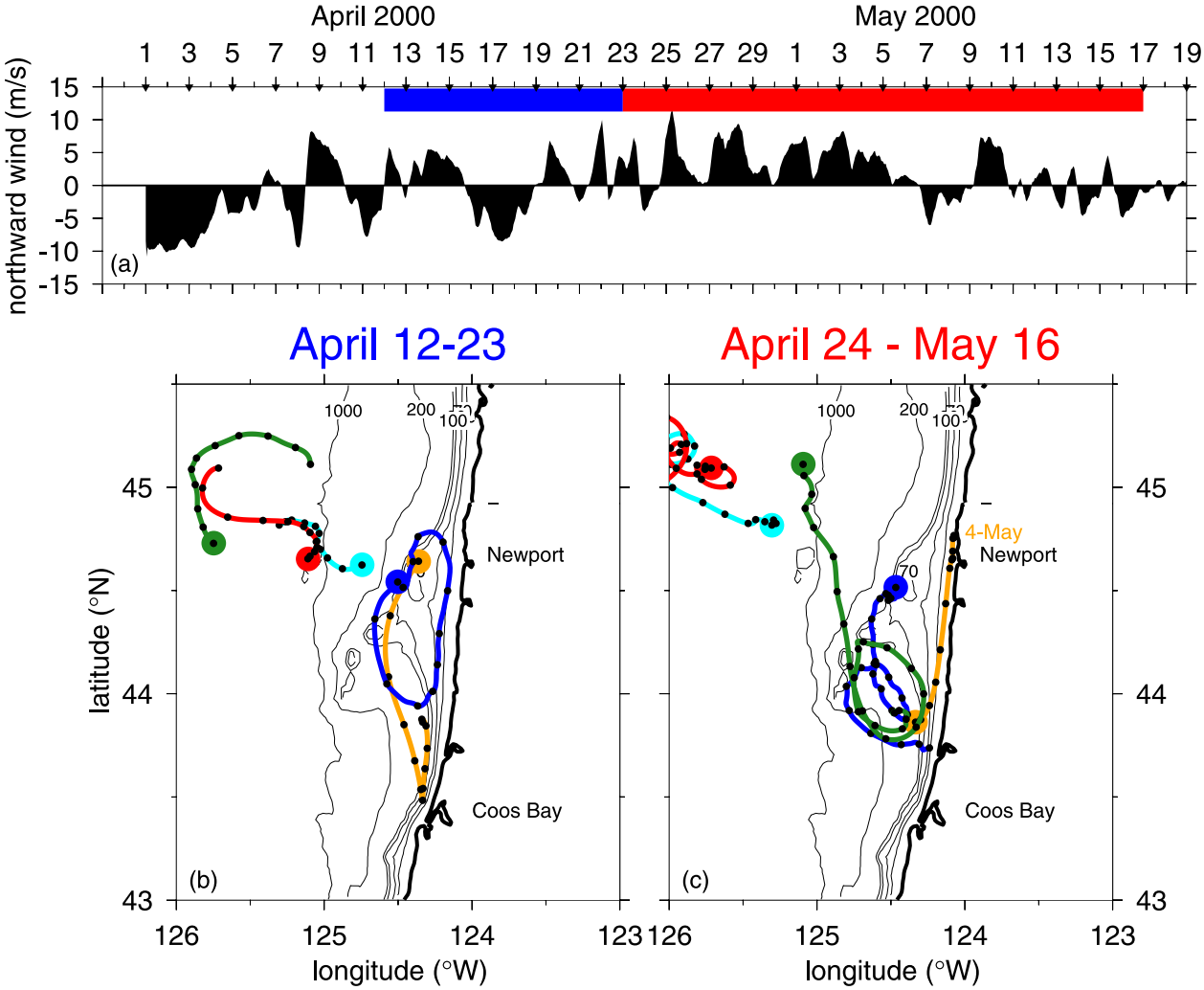

Figure 12. (a) North-south wind measured at NOAA NDBC buoy 46050 off Newport during spring 2000. (bottom) Trajectories of five surface drifters released along 44.6°N up to 65 nm offshore on 12 April 2000. Release locations are indicated by large filled color circles, and black dots are plotted once per day. From (b) 12 to 23 April the wind alternates between downwelling- and upwelling-favorable, but from (c) 24 April to 16 May it is predominantly to the north. In Figure 12c the large filled color circles are the drifter locations on 24 April.

influenced water, and a cool, subsurface inversion lying along the 25.7 kg m^{-3} density contour. This feature has been attributed to southward advection of cold Subarctic water in the coastal jet [*Huyer and Smith*, 1974]. A large region of cold water (7.75°–8°C) occupies three quarters of the water column downstream of Stonewall Bank. The 7.5°C isotherm intersects the bank summit and the cold, near-bottom water merges with the cool Subarctic inversion above. Note that the core of the coastal upwelling jet, located where the 25.7 kg m^{-3} isopycnal has the greatest slope (124.4°–124.6°W) is located on the offshore side of Stonewall Bank, consistent with the results described above.

[41] The buoyancy frequency field upstream of Stonewall Bank reveals a very stable surface layer, enhanced stratification in the upwelled seasonal pycnocline and relatively high stratification near the bottom (Figure 13, bottom). Downstream of the bank, regions of low stratification are observed over the bank summit and inshore. This is the region where the 7.5°C isotherms intersect the bottom and the large pool of 7.75°–8°C water is found in much of the water column. We interpret this pattern as due to mixing associated with wind-driven flow over the submarine bank bathymetry.

4. Discussion

[42] The separation of the equatorward coastal upwelling jet from the coast as it follows the widening midshelf isobaths defining the Heceta Bank complex off central Oregon is the key to the coastal ocean response in this region. This separation leads to many of the phenomena described above, most notably the creation of a low-velocity lee region inshore of the jet over the bank and the formation of alongshore pressure gradients. The low-velocity lee region is home to enhanced biological production and subsequent sinking of that material into a particle-rich bottom layer. The alongshore pressure gradients can drive

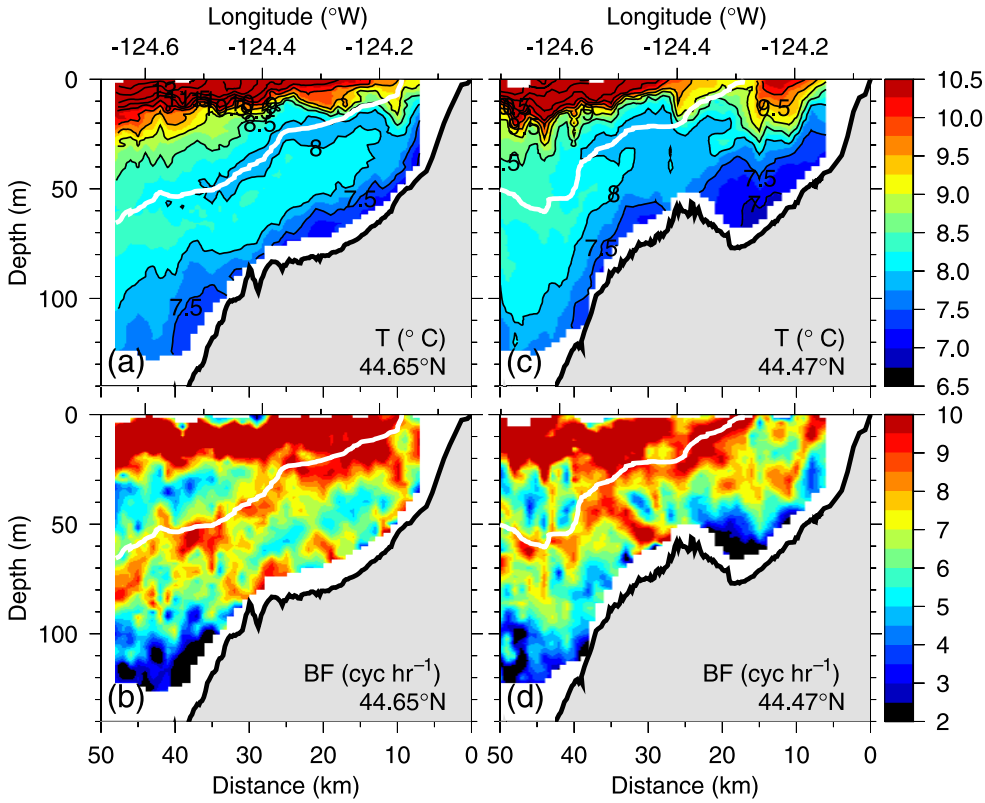

Figure 13. Vertical sections of (top) temperature and (bottom) buoyancy frequency from lines along (a, b) 44.65°N from 2254 UTC 27 July to 0218 UTC 28 July 1999 and (c, d) 44.47°N from 0522 to 1711 UTC 28 July 1999. The geographic location of these lines is indicated in Figure 6. The white contour in each panel is the 25.7 kg m^{-3} density contour.

northward flow when wind forcing relaxes, in particular near the coast and near the bottom over the mid shelf.

[43] As the jet approaches the southern end of the bank, it attempts to turn cyclonically back toward the coast to conserve potential vorticity. This is not fully accomplished, most likely because the wind-driven flow is too inertial for the flow to be able to adjust to the rapidly changing isobath orientation. The shelf break isobath (~200 m) turns 90° back to the east on the southern flank of the bank complex (Figure 1) in a very short distance. Thus the radius of curvature of the isobaths is on the scale of or less than the Rossby radius of deformation, about 5–7 km for the shelf flows considered here. Thus the Rossby number and the nonlinear terms in the momentum equation (i.e., the inertial terms) are expected to become important in this region. As wind energy is put into the system over the upwelling season, flow speeds in the time-dependent coastal upwelling jet vary, thus influencing the degree to which the jet is inertial. More details of the importance of the flow strength, as measured by the Rossby number of the flow, and the ratio of the Rossby radius of deformation to the radius of curvature of the bottom topography, i.e., a Burger number, on jet separation are explored by *Castelao and Barth* [2004].

4.1. Comparison With Other Regions

[44] The jet separation from the coast around Heceta Bank can be compared with coastal jet separation observed farther south in association with Cape Blanco, Oregon [*Barth et al.*, 2000]. The upstream geometry is fairly similar north of the Heceta Bank complex and north of Cape Blanco, i.e., a narrow continental shelf (Figure 1) over which lies a wind-driven, coastal upwelling jet. A major difference between the regions is that the coastline near Heceta Bank is fairly straight while Cape Blanco is a major coastal promontory. In addition, the shelf isobaths off Cape Blanco do not deviate from following the coastline to nearly the degree they do over Heceta Bank (Figure 1). Thus the baroclinic, approximately 100-m-deep coastal upwelling jet located over the mid to outer shelf is forced to adjust to major changes in bottom topography (Heceta Bank) or coastline curvature (Cape Blanco). Both lead to jet separation from the coast and, of critical importance for off-shelf transport, separation of the jet from the shelf.

[45] Before discussing more about the off-shelf flux associated with Heceta Bank, it should be noted that the wind fields differ dramatically between central Oregon and near Cape Blanco. Both the mean and variable components of alongshore wind stress just south of Cape Blanco increase by factors of 3–4 compared with near Heceta Bank [*Samelson et al.*, 2002]. Thus as suggested by *Samelson et al.* [2002] enhanced local wind forcing may be important in the jet separation process associated with Cape Blanco, although this remains to be fully investigated. What is clear, though, is that flow-topography interaction

dominates the separation process associated with Heceta Bank.

[46] The offshelf flux of coastal water and the material it contains into the adjacent deep ocean off the southern end of Heceta Bank is substantial. As noted above and reported in CB, the mean southward transport in the coastal jet over Heceta Bank and to the north (44°–45.2°N) is 0.66 and 0.44 Sv for spring and summer, respectively. For comparison, the offshelf surface Ekman transport from a 20 kt wind is 1.4 m^2 s^{-1}, so to equal a separating jet offshelf flux of 0.7 Sv would take 500 km of coastline or approximately from the southern end of Heceta Bank (44°N) to the Strait of Juan de Fuca. The cross-isobath transport at the southern end of the bank is responsible for fluxing a large amount of carbon off the shelf in the form of phytoplankton in an approximately 20-m-deep near-surface layer (Figures 4f and 4g). Quantification of this offshelf carbon flux using the velocity data and a regression between light attenuation and particulate organic carbon [*Karp-Boss et al.*, 2004] is the subject of a future paper. It is anticipated that this process could easily account for the large parcels of carbon of coastal origin observed farther offshore in the California Current System [*Barth et al.*, 2002]. Particulates from the deep, high light attenuation layer in the lee region of the bank could also be exported off the shelf by off-shelf deep currents. In particular, offshelf export could be accomplished on the inshore flank of the southward coastal upwelling jet which overlaps the deep particulate pool (e.g., from 124.55° to 124.7°W (Figures 4f and 4g)). This process would lead to the formation of midwater nephaloid layers offshore of the shelf break, evidence for which was found in deep CTD casts downstream of Heceta Bank (*O'Malley et al.* [2002], to be reported in a subsequent paper).

[47] The elements of flow-topography interaction that contribute to the productive fishery found over Heceta Bank can be compared with Georges Bank, another well-known, productive region off the east coast of North America. Georges Bank is a 150-km-wide, 280-km-wide topographic high that rises more than 100 m above the Gulf of Maine [*Uchipi and Austin*, 1987], roughly 2.5 times the linear dimensions of Heceta Bank. Georges Bank also has a significant effect on circulation over the continental shelf and slope and is a region of high biological production. Unlike the relatively highly stratified waters over Heceta Bank, Georges Bank waters are significantly mixed by tidal motion [*Garrett et al.*, 1978], which in part leads to the supply of nutrients into the euphotic zone and hence the bank's high biological production [*Horne et al.*, 1989]. Tidal rectification creates an important clockwise circulation around Georges Bank as strong tidal currents (up to 1 m s^{-1}) flow across isobaths as the semidiurnal-resonant Gulf of Maine fills and empties [*Loder*, 1980]. Tidally rectified flows are expected to be weak over Heceta Bank given the relatively weak barotropic tidal currents found there [*Erofeeva et al.*, 2003], but this phenomenon has not been adequately studied. As will be suggested below, the high production over Heceta Bank is due to the supply of nutrients via wind-driven upwelling to a region where currents are weak, and hence residence times are longer, i.e., the lee region created by the flow-topography interaction.

4.2. Ecosystem Consequences

[48] Flow-topography interaction as described above leads to elevated primary production over Heceta Bank. This elevated production is likely due to phytoplankton growth exceeding loss by horizontal advection of dilution by recently upwelled water with lower concentrations of phytoplankton. Elevated primary production fuels the coastal ecosystem as reflected by elevated levels of zooplankton [*Lamb and Peterson*, 2005] and fish, birds and whales [*Batchelder et al.*, 2002]. High production is also consistent with the highly successful fisheries in the Heceta Bank region [*Pearcy et al.*, 1989]. Lastly, mussel recruitment rates and phytoplankton concentration observed in the rocky intertidal are consistently higher inshore of the bank (Cape Perpetua, 44.25°N) than north of Heceta Bank (Cape Foulweather, 44.88°N) [*Menge et al.*, 2002]. The present research suggests that the lee region inshore over the Heceta Bank complex is conducive to high phytoplankton growth, which in turn may positively impact mussel recruitment in the rocky intertidal on the inshore side of Heceta Bank.

[49] Increased primary production over the bank, the subsequent sinking of that material to the bottom in the lee region of the bank and its subsequent respiration by microbial activity could lead to the formation of hypoxic bottom waters [*Wheeler et al.*, 2003; *Grantham et al.*, 2004]. The impact on higher trophic levels is particularly acute when this low-oxygen bottom water is forced into, and remains for several days in shallow water (<50 m depth) habitats which are home to rock fish and crabs [*Grantham et al.*, 2004].

[50] The pattern of time-dependent cross- and along-shelf circulation described here arising from flow-topography interaction over Heceta Bank has important consequences for the transport of larvae and particulates (phytoplankton and detritus) to and from the benthic coastal habitats off central Oregon. The motion of near-surface water parcels (northward during wind relaxation and reversal, onshore during northward winds) influences the supply of larvae to the coastal benthic habitat. In fact, temporal changes in barnacle recruitment are associated with cycles of upwelling and downwelling (B. A. Grantham et al., unpublished data, 1998).

4.3. Comparison With Circulation Models

[51] Many of the results presented here from in situ observations compare well with results from a numerical model study of this region by *Oke et al.* [2002b]. Using a periodic channel model extending from 43° to 46°N forced by observed winds and surface heat flux, *Oke et al.* [2002b] found that the circulation north of Heceta Bank, i.e., off Newport, is well described by classical upwelling theory. They also found that the coastal upwelling jet is deflected around Heceta Bank and the flow features they describe for southern Heceta Bank (an equatorward jet offshore near the Heceta Bank pinnacles and a second nearshore coastal upwelling jet, between which is found weak or reversed flow: compare Figures 4e and 4f with *Oke et al.* [2002b, Figure 8]; compare well with those described here and in CB. *Oke et al.* [2002b] use the model to show that the deep upwelled water inshore of the Heceta Bank pinnacles is drawn from the south during mid-July 1999 and is sometimes not connected with deep water to the north, again in

agreement with in situ observations presented in CB. Lastly, they used the numerical model to demonstrate that inshore of the coastal jet the acceleration of the alongshore flow is small and is driven by the difference between the surface stress and a negative alongshore pressure gradient. During wind relaxation, negative pressure gradients drive northward flow inshore on Heceta Bank as shown here.

[52] The creation of a negative alongshore pressure gradient to the south of a coastal promontory was attributed to flow-topography interaction by *Gan and Allen* [2002]. As the equatorward jet transits around the coastal cape, significant curvature vorticity is generated and the gradient wind balance requires greater upwelling of the isopycnals, hence colder, denser water (and low geopotential anomaly (see Figures 6 and 7)) being found downstream of the cape. This results in a negative alongshore pressure gradient in this region. The colder, upwelled water is fed by a geostrophically balanced onshore flow at depth. When wind forcing stops, the cross-shelf flow stops and the negative alongshore pressure gradient is unbalanced and thus drives flow to the north. This is the process that we suggests acts to drive the observed northward flows (Figure 8) from the observed alongshore geopotential anomaly gradient (Figures 6 and 7).

[53] *Kurapov et al.* [2005] use a numerical circulation model that assimilates currents from moorings deployed as part of COAST during summer 2001 to find good comparisons between model predictions and surface velocities from land-based coastal radar and hydrographic data from SeaSoar observations. They demonstrated that the complicated isopycnal structure on the southern flank of Heceta Bank (Figure 4e) was dramatically improved in the model when moored velocities from just a few current meter moorings were assimilated. *Kurapov et al.* [2005] further demonstrated that to accurately model the three-dimensional salinity field as measured by SeaSoar required the assimilation of moored salinity data because of the importance of advection of low-salinity, Columbia River–influenced water through the study region.

[54] Lastly, *Gan and Allen* [2005] extended the study of *Oke et al.* [2002b] by modeling a larger domain (41.7°–47.3°N) and using observed winds and surface heat fluxes from the COAST summer 2001 meteorological buoy to drive the model. Their results were similar to those of *Oke et al.* [2002b] including deflection of the coastal upwelling jet around Heceta Bank, a cyclonic turning of the jet as it transited the southern end of the bank, and negative pressure gradients driving northward flow inshore of the coastal upwelling jet during wind relaxation, all of which are seen in the observational data reported here. *Gan and Allen* [2005] also use detailed momentum and heat budgets as a function of depth and horizontal location to demonstrate the different balances between north of and over Heceta Bank.

4.4. Enhanced Mixing

[55] There is no evidence for the formation of tidal mixing fronts over Heceta Bank because of the strongly stratified summertime water column and the relatively weak tidal velocities. Nevertheless, the presence of wind-driven flow over Heceta and Stonewall Banks may lead to regions of enhanced mixing. *Ott et al.* [2004] show evidence for thick, turbulently mixed bottom layers on the inshore flank of the Heceta Bank pinnacles near 44.25°N. *Moum and Nash* [2000] report observations of turbulent bottom flow over Stonewall Bank where they estimate turbulent diffusivities are more than 100 times greater than over the continental shelf away from bottom topographic features. The results presented in section 3.7 suggest enhanced mixing near the bottom associated with equatorward flow over Stonewall Bank. The net influence of mixing near the bottom on details of the bottom boundary layer and the material it contains, and in providing drag on the wind-driven circulation is a subject for future investigation.

5. Conclusions

[56] The wind-driven coastal upwelling jet interacts strongly with the alongshore variations in bottom topography associated with the Heceta Bank complex off central Oregon. The structure of the hydrographic and velocity fields upstream of Heceta Bank over simple continental shelf bottom topography is well described by classical, two-dimensional upwelling models. As the midshelf upwelling jet and front encounter the bank topography rising to over 50% of the surrounding water column depth, the flow follows isobaths to the southwest, separating from the coastline. This results in a low-velocity "lee" region inshore on the bank complex that is an area of high primary production. As the strong coastal jet transits the southern end of the bank, it is unable to adjust rapidly enough to follow isobaths as they turn sharply back toward the coast. The coastal jet crosses the outer-shelf and upper-slope isobaths on the southern end of the bank resulting in large offshelf transport of water (of order 0.5–1.0 Sv) and the material it contains.

[57] By creating north-south variations in the normally purely east-west property gradients associated with coastal upwelling (e.g., temperature, density and geopotential anomaly), the flow-topography interaction creates north-south pressure gradients that can drive currents poleward during wind relaxation. This northward flow is found close to shore and at depth over the mid shelf (80–100 m water depth). During relaxation, the equatorward coastal upwelling jet still exists farther offshore, albeit weaker than during upwelling-favorable winds. The creation of alongshore pressure gradients by flow-topography interaction was documented during each of three upwelling seasons (1999–2001) and is thus a recurrent feature on the central Oregon coast. The alongshore pressure gradient could be monitored by moored instruments located upstream and over Heceta Bank. The locations of moorings deployed during the 2001 upwelling season are plotted in Figure 7. The creation, strength and time dependence of the alongshore pressure gradient could be related to both the resulting northward flows and to the wind strength, hence the intensity of the flow-topography interaction.

[58] The Oregon coastal ocean experiences strong downwelling-favorable (northward) winds several times during the typical spring-summer upwelling season. This results in onshore surface Ekman transport and downwelling of water and the material it contains (e.g., phytoplankton) within about 15 km of the coast. Associated with the downwelled isopycnals is a strong (>0.2 m s^{-1}) northward jet.

[59] Northward flow on the inshore side of the bank complex, either driven by alongshore pressure gradients or

directly forced by northward winds, provides the possibility for complete recirculation around the bank complex. As illustrated by surface drifters, water parcels may transit offshore along the outer edge of the bank before turning back toward the coast at the southern end of the bank and then can be entrained in the northward flow to return to the northern end of the bank complex. At this point, the parcels can be re-entrained in the southwestward flowing coastal upwelling jet. The time for complete recirculation is approximately 10 days.

[60] Finally, the flow-topography interaction results in a profound effect on the coastal ecosystem associated with Heceta Bank. High phytoplankton concentrations in the lee region inshore of the deflected coastal upwelling jet fuel a productive oceanic food chain. In turn, carbon from surface phytoplankton or in deep, bottom pools of organic matter can be fluxed off the shelf into the adjacent deep ocean by the separating coastal upwelling jet. The sinking of organic matter over the inshore side of the bank complex and its subsequent respiration is likely an important factor in the low-oxygen bottom waters observed there. An ecosystem model coupled to a circulation model and capable of determining oxygen production and consumption could be used to test hypotheses suggested by the observations reported here. For example, what is the balance between growth of phytoplankton versus loss through advection over the bank? With regard to the occurrence of hypoxic bottom waters, what is the relative contribution of low-oxygen source waters versus biological drawdown of oxygen through respiration? These and other questions await future study.

[61] **Acknowledgments.** We thank the officers and crew of the R/V *Wecoma* for their tireless efforts in towing SeaSoar on our survey grids while coexisting amicably with considerable fishing activity in this region. Oregon State University Marine Technicians M. Willis, L. Fayler, T. Martin, and D. Swensen were responsible for the highly successful SeaSoar operations. We thank R. O'Malley, A. Erofeev, and C. Wingard for their invaluable help with collecting, processing, and analyzing the voluminous data set presented here. G. Egbert and S. Erofeeva generously provided their tidal model of the region. The majority of this research was supported by the National Science Foundation grant OCE-9907854. The results reported from the 1999 Prediction of Wind-Driven Circulation project were supported by a National Oceanographic Partnership Program, Office of Naval Research grant N00014-98-1-0787, and those from the 2000 Global Ocean Ecosystem Dynamics Northeast Pacific Program were supported by NSF grants OCE-0001035 and OCE-0000733. R.C. was supported by the Brazilian government (CNPq, Conselho Nacional de Desenvolvimento Cientıacute;fico e Tecnológico, grant 200147/01-3) and by the Inter American Institute for Global Change Research (IAI) through project SACC (CRN-061).

References

Austin, J. A. (1998), Wind-driven circulation on a shallow, stratified shelf, Ph.D. thesis, 243 pp., Mass. Inst. of Technol./Woods Hole Oceanogr. Inst., Woods Hole, Mass.

Austin, J. A., and J. A. Barth (2002), Drifter behavior on the Oregon-Washington shelf during downwelling-favorable winds, *J. Phys. Oceanogr.*, *32*, 3132–3144.

Bane, J. M., M. D. Levine, R. M. Samelson, S. M. Haines, M. F. Meaux, N. Perlin, P. M. Kosro, and T. Boyd (2005), Atmospheric forcing of the Oregon coastal ocean during the 2001 upwelling season, *J. Geophys. Res.*, *110*, C10S02, doi:10.1029/2004JC002653.

Barth, J. A., and D. J. Bogucki (2000), Spectral light absorption and attenuation measurements from a towed undulating vehicle, *Deep Sea Res., Part I*, *47*, 323–342.

Barth, J. A., and P. A. Wheeler (2005), Introduction to special section: Coastal Advances in Shelf Transport, *J. Geophys. Res.*, *110*, C10S01, doi:10.1029/2005JC003124.

Barth, J. A., S. D. Pierce, and R. L. Smith (2000), A separating coastal upwelling jet at Cape Blanco, Oregon and its connection to the California Current System, *Deep Sea Res., Part II*, *47*, 783–810.

Barth, J. A., R. O'Malley, A. Y. Erofeev, J. Fleischbein, S. D. Pierce, and P. M. Kosro (2001), SeaSoar CTD observations from the Central Oregon Shelf, W9907C, 13–31 July 1999, *Data Rep. 184, Ref. 01-5*, 355 pp., Coll. of Oceanic and Atmos. Sci., Oreg. State Univ., Corvallis.

Barth, J. A., T. J. Cowles, P. M. Kosro, R. K. Shearman, A. Huyer, and R. L. Smith (2002), Injection of carbon from the shelf to offshore beneath the euphotic zone in the California Current, *J. Geophys. Res.*, *107*(C6), 3057, doi:10.1029/2001JC000956.

Barth, J. A., R. O'Malley, and A. Y. Erofeev (2003), SeaSoar observations during the Coastal Ocean Advances in Shelf Transport (COAST) Survey I: 23 May–13 June 2001, *Data Rep. 191, Ref. 03-1*, 670 pp., Coll. of Oceanic and Atmos. Sci., Oreg. State Univ., Corvallis.

Barth, J. A., S. D. Pierce, and T. J. Cowles (2005), Mesoscale structure and its seasonal evolution in the northern California Current system, *Deep Sea Res., Part II*, *52*, 5–28.

Batchelder, H. P., et al. (2002), The GLOBEC Northeast Pacific California Current System program, *Oceanography*, *15*, 36–47.

Bielli, S., P. Barbour, R. Samelson, E. Skyllingstad, and J. Wilczak (2002), Numerical simulations of the diurnal cycle along the Oregon coast during summertime northerly flow, *Mon. Weather Rev.*, *130*, 992–1008.

Butman, B., R. C. Beardsley, B. Magnell, D. Frye, J. A. Vermersch, R. Schlitz, R. Limeburner, W. R. Wright, and M. A. Noble (1982), Recent observations of the mean circulation on Georges Bank, *J. Phys. Oceanogr.*, *12*, 569–591.

Castelao, R. M., and J. A. Barth (2004), Wind-driven coastal circulation response to the presence of a shallow submarine bank, *Eos Trans. AGU*, *85*(47), Fall Meet. Suppl., Abstract OS32B-08.

Castelao, R. M., and J. A. Barth (2005), Coastal ocean response to summer upwelling favorable winds in a region of alongshore bottom topography variations off Oregon, *J. Geophys. Res.*, *110*, C10S04, doi:10.1029/2004JC002409.

Chase, Z., B. Hales, T. J. Cowles, R. Schwartz, and A. van Green (2005), Distribution and variability of iron input to Oregon coastal waters during the upwelling season, *J. Geophys. Res.*, *110*, C10S12, doi:10.1029/2004JC002590.

Cowles, T. J., J. A. Barth, C. E. Wingard, R. A. Desiderio, R. M. Letelier, and S. D. Pierce (2002), Mesoscale structure of bio-optical properties within the northern California Current System, 2000–2002, *Eos Trans. AGU*, *83*(47), Fall Meet. Suppl., Abstract OS62A-0226.

Daley, R. (1991), *Atmospheric Data Analysis*, 457 pp., Cambridge Univ. Press, New York.

Erofeeva, S. Y., G. D. Egbert, and P. M. Kosro (2003), Tidal currents on the central Oregon shelf: Models, data and assimilation, *J. Geophys. Res.*, *108*(C5), 3148, doi:10.1029/2002JC001615.

Gan, J., and J. S. Allen (2002), A modeling study of shelf circulation off northern California in the region of the Coastal Ocean Dynamics Experiment: Response to relaxation of upwelling winds, *J. Geophys. Res.*, *107*(C9), 3123, doi:10.1029/2000JC000768.

Gan, J., and J. S. Allen (2005), Modeling upwelling circulation off the Oregon coast during summer 2001, *J. Geophys. Res.*, *110*, C10S07, doi:10.1029/2004JC002692.

Garrett, C. J. R., J. R. Keeley, and D. A. Greenberg (1978), Tidal mixing versus thermal stratification in the Bay of Fundy and Gulf of Maine, *Atmos. Ocean*, *16*, 403–423.

Grantham, B. A., F. Chan, K. J. Nielsen, D. S. Fox, J. A. Barth, A. Huyer, J. Lubchenco, and B. A. Menge (2004), Upwelling-driven nearshore hypoxia signals ecosystem and oceanographic changes in the northeast Pacific, *Nature*, *429*, 749–754.

Hales, B., T. Takahashi, and L. Bandstra (2004), Atmospheric CO_2 uptake by a coastal upwelling system, *Global Biogeochem. Cycles*, *19*, GB1009, doi:10.1029/2004GB002295.

Hickey, B. M. (1997), The response of a steep-sided, narrow canyon to time-variable wind forcing, *J. Phys. Oceanogr.*, *27*, 697–726.

Horne, E. P. W., J. W. Loder, W. G. Harrison, R. Mohn, M. R. Lewis, B. Irwin, and T. Platt (1989), Nitrate supply and demand at the Georges Bank tidal front, *Sci. Mar.*, *53*, 145–158.

Huyer, A. (1990), Shelf circulation, in *Ocean Engineering Science*, vol. 9, *The Sea*, edited by B. LeMehaute and D. M. Haines, pp. 423–466, John Wiley, Hoboken, N. J.

Huyer, A., and R. L. Smith (1974), A subsurface ribbon of cold water over the continental shelf off Oregon, *J. Phys. Oceanogr.*, *4*, 381–391.

Huyer, A., R. L. Smith, and E. J. Sobey (1978), Seasonal differences in low-frequency current fluctuations over the Oregon continental shelf, *J. Geophys. Res.*, *83*, 5077–5089.

Huyer, A., R. L. Smith, and J. Fleischbein (2002), The coastal ocean off Oregon and northern California during the 1997–8 El Niño, *Prog. Oceanogr.*, *54*, 311–341.

Karp-Boss, L., P. A. Wheeler, B. Hales, and P. Covert (2004), Distributions and variability of particulate organic matter in a coastal upwelling system, *J. Geophys. Res.*, *109*, C09010, doi:10.1029/2003JC002184.

Kosro, P. M. (2005), On the spatial structure of coastal circulation off Newport, Oregon, during spring and summer 2001, in a region of varying shelf width, *J. Geophys. Res.*, doi:10.1029/2004JC002769, in press.

Kundu, P. K., and J. S. Allen (1976), Some three-dimensional characteristics of low-frequency current fluctuations near the Oregon coast, *J. Phys. Oceanogr.*, *6*, 181–199.

Kurapov, A. L., G. D. Egbert, J. S. Allen, and R. N. Miller (2003), M_2 internal tide off Oregon: Inferences from data assimilation, *J. Phys. Oceanogr.*, *33*, 1733–1757.

Kurapov, A. L., J. S. Allen, G. Egbert, R. Miller, P. M. Kosro, M. D. Levine, T. Boyd, J. A. Barth, and J. N. Moum (2005), Assimilation of moored velocity data in a model of coastal wind-driven circulation off Oregon: Multivariate capabilities, *J. Geophys. Res.*, *110*, C10S08, doi:10.1029/2004JC002493.

Lamb, J., and W. Peterson (2005), Ecological zonation of zooplankton in the COAST study region off central Oregon in June and August 2001 with consideration of retention mechanisms, *J. Geophys. Res.*, *110*, C10S15, doi:10.1029/2004JC002520.

Large, W. G., and S. Pond (1981), Open ocean momentum flux measurements in moderate-to-strong winds, *J. Phys. Oceanogr.*, *11*, 324–336.

Lentz, S. J. (1992), The surface boundary layer in coastal upwelling systems, *J. Phys. Oceanogr.*, *22*, 1517–1539.

Loder, J. W. (1980), Topographic rectification of tidal currents on the sides of Georges Bank, *J. Phys. Oceanogr.*, *10*, 1399–1416.

Menge, B. A., E. Sanford, B. A. Daley, T. L. Freidenburg, G. Hudson, and J. Lubchenco (2002), An inter-hemispheric comparison of bottom-up effects on community structure: Insights revealed using the comparative-experimental approach, *Ecol. Res.*, *17*, 1–16.

Moum, J. N., and J. D. Nash (2000), Topographically induced drag and mixing at a small bank on the continental shelf, *J. Phys. Oceanogr.*, *30*, 2049–2054.

Moum, J. N., D. M. Farmer, W. D. Smyth, L. Armi, and S. Vagle (2003), Structure and generation of turbulence at interfaces strained by internal solitary waves propagating shoreward over the continental shelf, *J. Phys. Oceanogr.*, *33*, 2093–2112.

Niiler, P. P., A. S. Sybrandy, K. Bi, P. M. Poulain, and D. Bitterman (1995), Measurement of the water-following capability of holey-sock and TRISTAR drifters, *Deep Sea Res., Part I*, *42*, 1951–1964.

Oke, P. R., J. S. Allen, R. N. Miller, G. D. Egbert, J. A. Austin, J. A. Barth, T. J. Boyd, P. M. Kosro, and M. D. Levine (2002a), A modeling study of the three-dimensional continental shelf circulation off Oregon. Part I: Model-data comparisons, *J. Phys. Oceanogr.*, *32*, 1360–1382.

Oke, P. R., J. S. Allen, R. N. Miller, and G. D. Egbert (2002b), A modeling study of the three-dimensional continental shelf circulation off Oregon. Part II: Dynamical analysis, *J. Phys. Oceanogr.*, *32*, 1383–1403.

O'Malley, R., J. A. Barth, and A. Y. Erofeev (2002), SeaSoar observations during the Coastal Ocean Advances in Shelf Transport (COAST) Survey II, W0108A: 6–25 August 2001, *Data Rep. 186, Ref. 02-2*, 537 pp., Coll. of Oceanic and Atmos. Sci., Oreg. State Univ., Corvallis.

Ott, M. W., J. A. Barth, and A. Y. Erofeev (2003), Microstructure measurements of a summer downwelling front, *Eos Trans. AGU*, *84*(46), Ocean Meet. Suppl., Abstract OS42M-07.

Ott, M. W., J. A. Barth, and A. Y. Erofeev (2004), Microstructure measurements from a towed undulating platform, *J. Atmos. Oceanic Technol.*, *21*, 1621–1632.

Pearcy, W. G., D. L. Stein, M. A. Hixon, E. K. Pikitch, W. H. Barss, and R. M. Starr (1989), Submersible observations of deep-reef fishes of Heceta Bank, Oregon, *Fish. Bull.*, *87*, 955–965.

Perlin, A., J. N. Moum, and J. Klymak (2005), Response of the bottom boundary layer over a sloping shelf to variations in alongshore wind, *J. Geophys. Res.*, *110*, C10S09, doi:10.1029/2004JC002500.

Pierce, S. D., and J. A. Barth (2002a), Acoustic Doppler current profiler observations during the Coastal Ocean Advances in Shelf Transport (COAST) Survey II: R/V Wecoma cruise W0108A, 6–25 August 2001, *Data Rep. 188, Ref. 02-4*, 106 pp., Coll. of Oceanic and Atmos. Sci., Oreg. State Univ., Corvallis.

Pierce, S. D., and J. A. Barth (2002b), Acoustic Doppler current profiler observations during the Coastal Ocean Advances in Shelf Transport (COAST) Survey I: R/V Wecoma cruise W0105C, 23 May to 13 June 2001, *Data Rep. 189, Ref. 02-5*, 129 pp., Coll. of Oceanic and Atmos. Sci., Oreg. State Univ., Corvallis.

Pollard, R. T. (1986), Frontal surveys with a towed profiling conductivity/temperature/depth measurement package (SeaSoar), *Nature*, *323*, 433–435.

Reinsch, C. H. (1967), Smoothing by spline functions, *Numer. Math.*, *10*, 177–183.

Samelson, R., P. Barbour, J. Barth, S. Bielli, T. Boyd, D. Chelton, P. Kosro, M. Levine, and E. Skyllingstad (2002), Wind stress forcing of the Oregon coastal ocean during the 1999 upwelling season, *J. Geophys. Res.*, *107*(C5), 3034, doi:10.1029/2001JC000900.

Smith, R. L. (1981), A comparison of the structure and variability of the flow field in three coastal upwelling regions: Oregon, northwest Africa, and Peru, in *Coastal Upwelling*, *Coastal Estuarine Ser.*, vol. 1, edited by F. A. Richards, pp. 107–118, AGU, Washington, D. C.

Spitz, Y. H., J. S. Allen, and J. Gan (2003), Comparison of two- and three-dimensional simulations of the ecosystem response to upwelling off the Oregon coast, *Eos Trans. AGU*, *84*(46), Ocean Meet. Suppl., Abstract OS52I-06.

Strickland, J. D. H., and T. R. Parsons (1972), *A Practical Handbook of Sea Water Analysis*, *Bull. 167*, 310 pp., Fish. Res. Board of Can., Ottawa.

Torgrimson, G. M., and B. M. Hickey (1979), Barotropic and baroclinic tides over the continental slope and shelf off Oregon, *J. Phys. Oceanogr.*, *9*, 945–961.

Trowbridge, J. H., and S. J. Lentz (1991), Asymmetric behavior of an oceanic boundary layer above a sloping bottom, *J. Phys. Oceanogr.*, *21*, 1171–1185.

Uchipi, W., and J. A. Austin Jr. (1987), Morphology, in *Georges Bank*, edited by J. H. Ryther and J. W. Farrington, pp. 25–30, MIT Press, Cambridge, Mass.

WET Labs Inc. (1997), FlashPak user's guide, internal report, 16 pp., Philomath, Oreg.

Wheeler, P. A., A. Huyer, and J. Fleischbein (2003), Cold halocline, increased nutrients and higher chlorophyll off Oregon in 2002, *Geophys. Res. Lett.*, *30*(15), 8021, doi:10.1029/2003GL017395.

J. A. Barth, R. M. Castelao, and S. D. Pierce, College of Oceanic and Atmospheric Sciences, 104 COAS Admin Building, Oregon State University, Corvallis, OR 97331-5503, USA. (barth@coas.oregonstate.edu; castelao@coas.oregonstate.edu; spierce@coas.oregonstate.edu)